Performance of Scattering Matrix Decomposition and Color Spaces for Synthetic Aperture Radar Imagery.

THESIS

Manuel E. Arriagada, Captain, Chilean Air Force

AFIT/GE/ENG/10-03

DEPARTMENT OF THE AIR FORCE
AIR UNIVERSITY

AIR FORCE INSTITUTE OF TECHNOLOGY

Wright-Patterson Air Force Base, Ohio

The views expressed in this thesis are those of the author and do not reflect the official policy or position of the United States Air Force, Chilean Air Force, Department of Defense, Chilean Ministry of Defense, the United States Government or Chilean Government.

AFIT/GE/ENG/10-03

Performance of Scattering Matrix Decomposition and Color Spaces for Synthetic Aperture Radar Imagery.

THESIS

Presented to the Faculty

Department of Electrical and Computing Engineering

Graduate School of Engineering and Management

Air Force Institute of Technology

Air University

Air Education and Training Command

In Partial Fulfillment of the Requirements for the

Degree of Master of Science

Manuel E. Arriagada, Bach.Eng.

Captain, Chilean Air Force

March 2010

AFIT/GE/ENG/10-03

Performance of Scattering Matrix Decomposition and Color Spaces for Synthetic Aperture Radar Imagery.

Manuel E. Arriagada, Bach.Eng.
Captain, Chilean Air Force

Approved:

Maj Michael A. Saville, PhD Committee Chair	Date
Dr. Michael A. Temple Committee Member	Date
Dr. Andrew J. Terzuoli Committee Member	Date

Abstract

Polarimetrc Synthetic Aperture Radar (SAR) has been shown to be a powerful tool in remote sensing because uses up to four simultaneous measurements giving additional degrees of freedom for processing. Typically, polarization decomposition techniques are applied to the polarization-dependent data to form colorful imagery that is easy for operators systems to interpret. Yet, the presumption is that the SAR system operates with maximum bandwidth which requires extensive processing for near- or real-time application. In this research, color space selection is investigated when processing sparse polarimetric SAR data as in the case of the publicly available "Gotcha Volumetric SAR Data Set, Version 1.0". To improve information quality in resultant color imagery, three scattering matrix decompositions were investigated (linear, Pauli and Krogager) using two common color spaces (RGB, CMY) to determine the best combination for accurate feature extraction. A mathematical model is presented for each decomposition technique and color space to the Crámer-Rao lower bound (CRLB) and quantify the performance bounds from an estimation perspective for given SAR system and processing parameters. After a deep literature review in color science, the mathematical model for color spaces was not able to be computed together with the mathematical model for decomposition techniques. The color spaces used for this research were functions of variables that are out of the scope of electrical engineering research and include factors such as the way humans sense color, environment influences in the color stimulus and device technical characteristics used to display the SAR image. Hence, SAR imagery was computed for specific combinations of decomposition technique and color space and allow the reader to gain an abstract view of the performance differences.

Acknowledgements

Before all, to my wife, your support, comfort, motivation and understanding beyond any reasonable circumstances was the strength that always pushes me to be better every day as a husband, father and student. To my beautiful son, who was able to turn any bad day into a happy day just with a smile. Thank you both for all the sacrifices that you went through during our life far from our home country. To my parents, the family values and the education that you provide to me in my early years were the foundation to build what I am now. Thank you both for all the support that you always have given to me and my family. To the Chilean Air Force and the Republic of Chile, who trust in my person for this Master program. To the staff of the AFIT IMSO office and the Family Support, who provides continuous support to my family, I can't imagine going through all this without your help. To my classmates, who were always there to offer me a hand when I was lost behind the barriers of the language or the knowledge. To the faculties who give me the tools to build this project and provide feedback that helps to maintain the right direction, specially to my research advisor who always was pushing my own limits to go further and be better.

Manuel E. Arriagada

Table of Contents

Page

List of Figures

List of Tables

List of Symbols

List of Abbreviations

Performance of Scattering Matrix Decomposition and Color Spaces for Synthetic Aperture Radar Imagery.

I. Introduction

1.1 Research Motivation

Synthetic aperture radar (SAR) is an active radio frequency (RF) imaging technique that utilizes signal processing to produce high quality images. SAR systems gather information about a target area's reflectivity when illuminated by an electromagnetic (EM) wave at a specific radio frequency and from a particular aspect angle. Sequential observations of the target area, or scene, over varying aspect angles are processed to produce an estimate of the scene's reflectivity which is viewed similar to a photographic image. EM waves propagate virtually unattenuated through most atmospheric conditions enabling SAR to provide an all weather, day/night imaging capability.

To deliver information in real time, it is very important to present the information in a way that the system or operator can quickly, easily and accurately identify important features. Synthetic Aperture Radar (SAR) has shown to be an efficient technology for getting visual representation of a target or area of interest and the all weather capability of SAR is an invaluable characteristic that makes this technology useful at any time [27].

As the target for SAR is the ground clutter, SAR applications include cartography, land use analysis, and oceanography in civil applications of remote sensing (RS). Military applications include surveillance, reconnaissance, battle damage assessment, ground target classification and navigation. SAR technology can generate imagery with a wide range of resolution, but the typical products are monochrome images which are estimates of the scalar quantity of reflectivity [13]. By using a system capable of measuring the four combinations of polarization (HH, HV, VH and VV,

where the first component as the transmitted polarization and the second component as the received polarization), we can get four different views from the same scene and combine them into a multi-colored image. With color intensity being proportional to some combination of the polarizations, a trained operator can gain additional insight beyond just spatial arrangement. Of course, the amount of added value is subjective as each person views color differently.

Furthermore, advances in high performance computing (HPC) enable near-real time processing, but when HPC is not available, one must make a trade-off between SAR image resolution and processing time. So, one might ask: What are the trade-offs between image resolution and processing time in consideration of how the human operator interprets multi-color imagery? In other words, can multi-color imagery make up for lost resolution? Hence, this thesis investigates the quality of multi-color SAR imagery when applied to sparse SAR data.

Polarimetric SAR dates back to the 1940's when Sinclair, Kennaugh and Huynen introduced methods to use polarized radar echoes to characterize aircraft targets [16]. The capability of a polarimetric SAR system to obtain the four different polarization channels give us four different views of the same area of interest or target. This characteristic allow the exposition of many of the features when the four different views are combined. At the same time, this characteristic allows the detection of the polarimetric signature of a particular target scatterer which is a helpful tool for target recognition. Several decomposition techniques of the target matrix have been developed. For this thesis, the linear, the Pauli and the Krogager are analyzed using signal processing tools available and using data from the "Gotcha Volumetric SAR Data Set, Version 1.0". This data set was prepared and provided by the United States Air Force Research Laboratory (AFRL) [4].

The "Gotcha Volumetric SAR Data Set, Version 1.0" has been used to investigate 2-D and 3-D imaging of stationary targets from wideband, fully polarimetric data. To capture the urban scene consisting of civilian vehicles and calibration tar-

gets, the SAR operated in the circular mode and completed 8 circular orbits around the scene at incremented altitudes. The distributed data included phase history data, auxiliary data, processed images, ground truth pictures and a collection summary report making it an ideal set to investigate the scattering matrix decomposition and multi-color processing.

The goal for this research is to highlight features that allow operators to quickly identify targets of interest for a desired level of confidence. Hence, three popular scattering matrix decomposition techniques are applied to two different color spaces to determine the best combination for target feature extraction.

1.2 Research Scope and Assumptions

SAR imagery is widely used for a broad spectrum of applications. From cartography, geology, oceanography, agriculture to a surveillance, reconnaissance and target recognition. This research is focused in use imagery as a tool to extract features from objects present in the scene in a way that is easy for an operator of any system with SAR imagery to recognize objects of interest. In order to work with real data, the "Gotcha Volumetric SAR Data Set, Version 1.0" is used to compute imagery with information of the four polarization channels available in this data set. As described in section 1.1, the "Gotcha Volumetric SAR Data Set, Version 1.0" is data from a fully polarimetric SAR system and collected from a parking lot which contains some calibration targets such as a top hat, a trihedral, a dihedral, and different types of passenger cars. The method of collecting this data was by spotlight collection. The platform made eight passes around the target.

The scope of this research is to compute three decomposition techniques used in SAR polarimetry (linear, Pauli and Krogager), each of them in two different color spaces (RGB and CMY), with the aim of comparing them and establishing a metric that allows us to determine the best combination for an operator to see features more efficiently and accurately. The metric proposed is the Crámer-Rao Lower Bound

and the SAR data set is the "Gotcha Volumetric SAR Data Set, Version 1.0". The assumptions are that color spaces are able to be compared in a mathematical sense and that can be computed in a signal model that will depend on the decomposition technique to be used. The data set is a sparse data set. The results will be provided taking into account that the SAR system is not high resolution and that the extracted information is not high quality.

1.3 Document Overview

This document details the polarimetric theory and methodology from a performance point of view. Chapter II is an introduction to polarimetric SAR imaging considering Polarimetric SAR fundamentals, Scattering matrix and describing some airborne and space polarimetric SAR systems. Colorimetry is also introduced in this chapter, presenting the fundamentals of the RGB and CMY color spaces, defined for this research. Next, Chapter III introduce the two decomposition techniques that are considered on this research and the relationship of this technology and Colorimetry, as well as a description of the Crámer-Rao Lower Bound that is considered as a way to obtain a metric of performance between each decomposition technique. In chapter IV the results of this research are discussed in order to present final results, conclusions and contributions of this research in chapter V.

II. Synthetic Aperture Radar Imaging

2.1 Synthetic Aperture Radar.

SAR is perhaps one of the most efficient technologies for getting a visual representation of a target or an area of interest. The all weather capability of SAR is an invaluable characteristic that makes this technology useful at any moment. Today, SAR applications drive continual system development that allows researchers to extract more features out of the measured data. Special SAR applications are forward looking SAR, measurement of object height, foliage-penetration, ground mapping, target recognition, and surveillance, to name a few.

2.2 Radar Imaging.

An image is probably the best way to deliver information to a decision making machine or an operator. For the human being, vision is one of the primary and perhaps the most important sensor. The eye collects the light reflected by objects in the surrounding medium and transforms the energy into information for the human being to decide how to interact with the environment. The invention of the Synthetic Aperture Radar changed the way humans sense the environment because it provides the same capability without light or a direct visual line-of-sight (LOS). The main goal of SAR is to improve focusing by synthesizing a huge lens in what is called synthetic aperture [19, 22, 24, 27]. In order to obtain an image of a particular area or target, an airborne SAR operates in different modes. The more traditional SAR modes are: Spotlight and Strip map. The Spotlight SAR mode utilizes a mechanical or electronically steering of a physical radar antenna. The purpose of the beam steering is to irradiate a finite target area centered in a particular point in the spatial domain as the radar is moved along a straight line. This beam maintains the physical radar radiation pattern in the same target area while the platform moves along the synthetic aperture. In the Strip map SAR mode, the antenna maintains a fixed radiation pattern throughout the data acquisition period. For such a data collection

scheme, the illuminated cross-range area is varied from one pulse transmission to the next. This mode is mainly used for reconnaissance or surveillance problems.

2.2.1 Synthetic Aperture Radar (SAR) Imaging. The target for SAR is the ground clutter. Due to this characteristic, SAR applications include cartography, land analysis and oceanography in the civilian side. This activity is known as Remote Sensing (RS). In the military, surveillance, battle damage assessment, reconnaissance, ground target classification and navigation are also performed by SAR systems. SAR technology is applied from airborne and space platforms and can generate images with a wide range of resolutions. What SAR produces is a monochrome image relative to a measurement of the scene reflectivity. The all weather characteristic of SAR imaging makes this technology an important and efficient tool with better performance than optical imaging systems during inclement weather.

2.2.2 Polarimetric SAR. SAR polarimetry provides data about the polarization state of the returned signal for every resolution element or pixel, which complements the intensity information from the target return. SAR polarimetry is achieved by measuring two orthogonally polarized waves. Typically for each transmission, the radar simultaneously receives two orthogonally polarized waves. These waves can be processed by range and azimuth correlation. The relative phases of the received voltages are measured by using phase coherence of transmitted signals and coherent addition on received signals [16, 19, 22, 28].

2.2.2.1 Polarization State. The polarization state of an electromagnetic wave can be illustrated using the polarization ellipse. In Figure 2.1, we observe the projection of the electric field vector on to the x-y plane when traveling in z-direction [16, 22]. We can also describe the polarization state of the wave by using the two Stokes parameters ψ (orientation angle) and χ (ellipticity angle) [22, 23]. In this case, right hand circular polarization is given by $\chi = -45^o$, left hand circular polarization is given by $\chi = +45^o$. The normalized Stokes vector of an electromagnetic

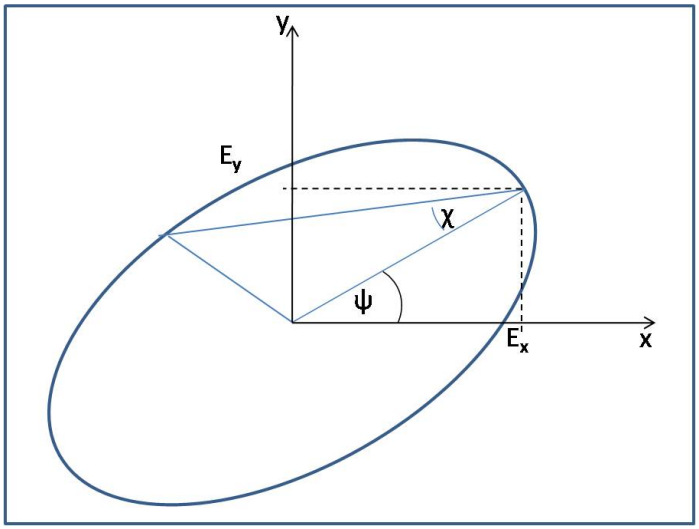

Figure 2.1: Polarization Ellipse [22].

wave is given by:

$$\begin{aligned} S_0 &= 1.0 \\ S_1 &= \cos(2\psi)\cos(2\chi) \\ S_2 &= \sin(2\psi)\cos(2\chi) \\ S_3 &= \sin(2\chi) \end{aligned} \tag{2.1}$$

The power, and thus the pixel intensity value can be calculated from the Stokes matrix of the resolution element and the stokes vector for transmitter receiver polarizations:

$$\text{Power} = K[S_r]^T[M][S_1] \tag{2.2}$$

where :

$[S_r]$ = Stokes vector of the receiver;

$[M]$ = Stokes matrix of the resolution element;

$[S_1]$ = Stokes vector of the transmitter;

K = constant factor normalized to 1;

With the stokes matrix defined, we can vary four parameters independently: the receiver orientation ψ_r and ellipticity χ_r, and transmitter orientation ψ_t and ellipticity χ_t. Due to these considerations, the power received and the pixel intensity value are functions of four variables $(\psi_r, \chi_r, \psi_t, \chi_t)$. From the information contained in the Stokes matrix, we can code pixel intensity values with the combinations between transmitter and receiver polarization, encoding the received power for each pixel as a gray value.

2.2.3 Representation of Polarimetric SAR Data. In order to represent polarimetric SAR data, various scattering vectors will be presented. Alternative ways of describing waves that span a range of frequencies are necessary. Considering that we introduce the coherency vector and the Stokes vector. In addition to being useful for multi-frequency waves, the stokes vector helps to the understanding of the Poincaré sphere, by which the polarization of a single-frequency wave can be represented graphically.

2.2.3.1 Coherency Vector. Consider a single frequency plane wave traveling in the z direction of a right handed coordinate system. The coherency vector of the wave is defined as:

$$J = E \otimes E^* \tag{2.3}$$

where * denotes the complex conjugate and $\otimes$ denotes the Kronecker product or direct product, defined for two-element vectors by:

$$A \otimes B = \begin{bmatrix} A_1 B \\ A_2 B \end{bmatrix} = \begin{bmatrix} A_1 B_1 \\ A_1 B_2 \\ A_2 B_1 \\ A_2 B_2 \end{bmatrix} \tag{2.4}$$

2.2.3.2 The Stokes Vector. Considering that the elements of the coherency vector are complex values and that Stokes proposes four parameters to characterize the amplitude and polarization of a wave, the parameters can be arranged in a vector form, also known as Stokes vector G, which is a transform of the coherency vector [9, 16, 22]:

$$G = QxJ \tag{2.5}$$

where:

$$Q = \begin{bmatrix} 1 & 0 & 0 & 1 \\ 1 & 0 & 0 & -1 \\ 0 & 1 & 1 & 0 \\ 0 & j & -j & 0 \end{bmatrix} \tag{2.6}$$

The elements of the Stokes vector are:

$$G_0 = |E_x|^2 + |E_y|^2 \tag{2.7}$$

$$G_1 = |E_x|^2 - |E_y|^2 \tag{2.8}$$

$$G_2 = 2\,|E_x|\,|E_y| \cos\phi \tag{2.9}$$

$$G_3 = 2\,|E_x|\,|E_y| \sin\phi \tag{2.10}$$

where ϕ is the phase difference between the y and x components of the wave. Amplitude and polarization of a wave can be described by the Stokes vector, where the parameter G_o gives the amplitude, $|E_x|$ and $|E_y|$ can be derived from G_0 and G_1 and the phase ϕ can be determined from either G_2 and G_3. Further derivations can be found in [22].

2.2.3.3 The Poincaré Sphere. According to [22], as shown on Figure 2.2, G_1, G_2 and G_3 can be considered Cartesian coordinates of a point on a sphere of radius G_0 and 2ε and 2τ can be considered latitude and azimuth angles measured

to the point. This interpretation is known as Poincaré Sphere and was introduced by Poincaré. With this model, a single-frequency wave is described by a point on the Poincaré sphere. There is a point of the sphere for every state of polarization and vice-versa.

2.2.3.4 Special Points on the Poincaré Sphere. The point on the Poincaré sphere corresponding to $|E_x| = |E_y|$, $\phi = \pi/2$, $G_1 = G_2 = 0$, and $G_3 = G_0$ represents the north pole (+ z axis) of the Poincaré sphere and left-hand-circular polarization. The point corresponding to$|E_x| = |E_y|$, $\phi = -\pi/2$, $G_1 = G_2 = 0$, and $G_3 = -G_0$ represents the south pole and right-handed-circular wave. For a left-handed-elliptic wave, $0 < \phi < \pi$ and $G_3 > 0$. For this case all points are plotted in the upper hemisphere.

For a right-handed-elliptic wave, $\pi < \phi < 2\pi$ and $G_3 > 0$. For this case all points are located in the lower hemisphere. For linear polarization, points are located at the equator, at the $-x$-axis intersection with the sphere for linear left vertical polarization; at the $+x$-axis intersection for linear horizontal. The $+y$-axis corresponds to linear polarization with a tilt angle of $\pi/4$, and the $-y$-axis to linear polarization with a tilt angle of $-\pi/4$.

2.2.4 Radar Polarimetry. This operating principle is based on the quasi-simultaneous transmission of two linear orthogonal waves. Upon reception, the echoes are received by two linear and orthogonal polarized antennas which have the same phase reference. Assuming that at a given instant the radar transmits in the $\hat{k}^{inc}$ direction a pulse whose polarization $\hat{E}_0^{inc1}$ is directed along the $\hat{x}$-axis, the target backscatters along the direction $\hat{k}^s$ an electric field $\vec{E}_0^{s1}$ whose direction is unknown. However two components of this scattered field, namely $\hat{z} \cdot \vec{E}_0^{s1}$ and $\hat{t} \cdot \vec{E}_0^{s1}$, will be collected on the two receiving polarizations directed along the $\hat{z}$ and $\hat{t}$ directions. A moment later, a field described by the Jones vector $\hat{E}_0^{inc2}$ oriented along the $\hat{y}$ axis is transmitted. Similarly, the components $\hat{z} \cdot \vec{E}_0^{s2}$ and $\hat{t} \cdot \vec{E}_0^{s2}$ are collected. The main

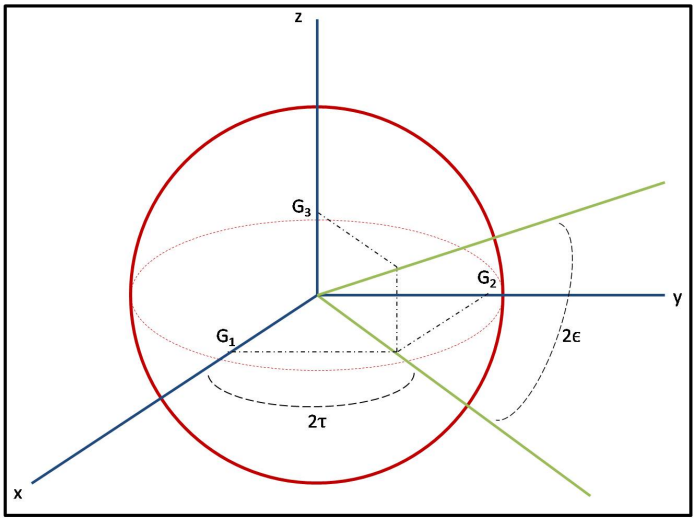

Figure 2.2: Poincaré Sphere [19, 22].

constraint in polarimetric measurements comes from the need to transmit two phase-locked waveforms with orthogonal polarizations. It requires to transmit interleaved pulses, alternating polarization after each transmitted pulse ($\hat{x}, \hat{y}, \hat{x}, \hat{y}, etc.$). Each collected echo requires the recording of two signals, each one associated with one of the receiving polarizations. That means double polarization agility. If we want to maintain a performance for each channel similar to a single polarized radar with azimuth sampling frequency f_a, the polarimetric radar must operate at $2f_a$. As a consequence of doubling both sampling frequency and reception modes, the volume of data generated per image pixel is increased by a factor of four. Another consequence is that the radar's swath width is reduced by a factor of two in order to protect the receiver against range ambiguities. The antenna width is multiplied by a factor of two (and thus so is its surface), while the total transmitted power may remain the same. In conclusion, the polarimetry option involves multiplying the volume of data per image pixel by four and halving the swath width, which are heavy constraints that tend to argue against polarimetry. A compact polarimetric architecture can relieve these intrinsic constraints.

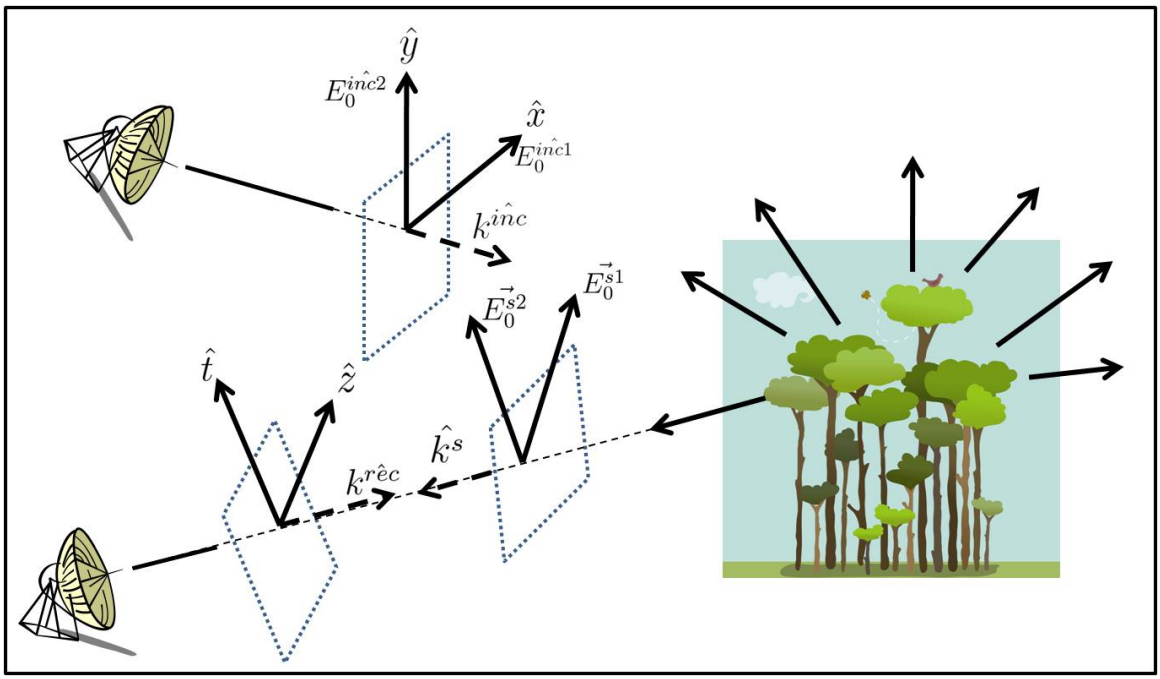

Figure 2.3: Principle of Radar Polarimetry [19].

2.2.5 The Scattering Matrix. The information stored in matrix form for each pixel of a polarimetric SAR image is described by the scattering matrix [16, 19]:

$$\left[\overline{\overline{S}}\right] = \begin{bmatrix} S_{xz} & S_{yz} \\ S_{xt} & S_{yt} \end{bmatrix} = \begin{bmatrix} \widehat{z} \cdot \vec{E}_0^{s1} & \widehat{z} \cdot \vec{E}_0^{s2} \\ \widehat{t} \cdot \vec{E}_0^{s1} & \widehat{t} \cdot \vec{E}_0^{s2} \end{bmatrix} \tag{2.11}$$

where $\overline{\overline{S}}$ is the scattering matrix. The indices i and j of the complex coefficients S_{ij} indicate transmission modes (x or y) and reception modes (z or t). The polarization basis of ($\widehat{x}$ or $\widehat{y}$) and ($\widehat{z}$ or $\widehat{t}$) are oriented according to the Back Scattering Alignment convention (BSA). The advantage of BSA is that ($\widehat{x}$,$\widehat{y}$) and ($\widehat{z}$,$\widehat{t}$) are identical in a monostatic configuration of our polarization SAR system [19, 22]. Considering $\left[\overline{\overline{S}}\right]$, the response of the target to any elliptical polarization of Jones vector $\widehat{t} \cdot \vec{E}_0^{inc}$ can be computed immediately. $\widehat{t} \cdot \vec{E}_0^{inc}$ is indeed the linear combination of two waves with linear orthogonal polarizations $\widehat{x}$ and $\widehat{y}$ [19]:

$$\widehat{E}_0^{inc} = \left(\widehat{x} \cdot \widehat{E}_0^{inc}\right) \cdot \widehat{x} + \left(\widehat{y} \cdot \widehat{E}_0^{inc}\right) \cdot \widehat{y} = E_0^{inc} \cdot \widehat{x} + E_0^{inc} \cdot \widehat{y} \tag{2.12}$$

from which, assuming the linearity of the measurement process described by

$$\begin{bmatrix} E^s_{0z} \\ E^s_{0t} \end{bmatrix} = \begin{bmatrix} S_{xz} & S_{yz} \\ S_{xt} & S_{yt} \end{bmatrix} \begin{bmatrix} E^{inc}_{0x} \\ E^{inc}_{0y} \end{bmatrix} \tag{2.13}$$

E^{inc}_{0x} and E^{inc}_{0y} are the components of the incident field (i.e., the incident Jones vector) $\widehat{E}^{inc}_0$ expressed in the transmission basis ($\widehat{x}$,$\widehat{y}$); E^s_{0z} et E^s_{0t} are those of the scattered field (i.e. the scattered Jones vector) $\vec{E}^s_{0x}$ expressed in the reception basis ($\widehat{z}$,$\widehat{t}$). Equation (2.13) relates Jones vectors of the transmitted and scattered waves. In other words, we are able to characterize the target by its ability to modify the polarization of the illumination wave. For this research, a monostatic configuration for a SAR system is considered, since the same antenna transmits and receives. As a result, we can say:

$$\widehat{z} = \widehat{x} \qquad \widehat{t} = \widehat{y} \qquad \widehat{k}^{rec} = \widehat{k}^{inc} = -\widehat{k}^s \tag{2.14}$$

where $\widehat{k}^{rec}$ is the wave vector of the receiving polarization. If the background media is simple linear isotropic and homogeneous, the wave propagation between the radar and the ground does not contribute the off-diagonal terms of $\overline{\overline{S}}$ which simplifies to the backscattering matrix [19]:

$$S_{yx} = S_{xy} \tag{2.15}$$

Considering Eq. 2.15, the backscattering matrix is a complex diagonal square matrix, defined by three amplitude values and three phase values. If we factor out the absolute phase S_{xx} the number of independent parameters is reduced to five, three amplitude values and two phase difference values:

$$\begin{aligned} \left[\overline{\overline{S}}\right] &= \begin{bmatrix} S_{xx} & S_{yx} \\ S_{xy} & S_{yy} \end{bmatrix} \\ &= e^{j\phi_{xx}} \begin{bmatrix} |S_{xx}| & |S_{xy}|\, e^{j(\phi_{xy}-\phi_{xx})} \\ |S_{xy}|\, e^{j(\phi_{xy}-\phi_{xx})} & |S_{yy}|\, e^{j(\phi_{yy}-\phi_{xx})} \end{bmatrix} \end{aligned} \tag{2.16}$$

Now we can apply the following substitutions, where $\widehat{x}$ is replaced by $\widehat{h}$ for horizontal direction, and $\widehat{y}$ is replaced by $\widehat{v}$ for vertical direction, as follows:

$$S_{xx} = S_{hh},\ S_{yy} = S_{vv},\ S_{xy} = S_{hv}$$

2.2.6 Polarimetric SAR Implementation. The polarimetric SAR implementation used for this analysis is described as follows:
Using the linear polarization, the scattering vector $\overline{k}_L$ can be written as:

$$\overline{k}_L = \begin{bmatrix} S_{hh} \\ \sqrt{2}S_{hv} \\ S_{vv} \end{bmatrix} \tag{2.17}$$

where S_{xy} means the scattering response when a transmit electromagnetic wave is y-polarized while the receive antenna is x-polarized. Using the Pauli matrix basis, we have a coherent scattering vector described as $\overline{k}_P$:

$$\overline{k}_P = \frac{1}{\sqrt{2}} \begin{bmatrix} S_{hh} + S_{vv} \\ 2S_{hv} \\ S_{vv} - S_{hh} \end{bmatrix} \tag{2.18}$$

Using a circular polarization basis, we have a coherent scattering vector described as $\overline{k}_C$:

$$\overline{k}_C = \frac{1}{2} \begin{bmatrix} S_{hh} - S_{vv} + 2iS_{hv} \\ S_{hh} + S_{vv} \\ S_{hh} - S_{vv} - 2iS_{hv} \end{bmatrix} \tag{2.19}$$

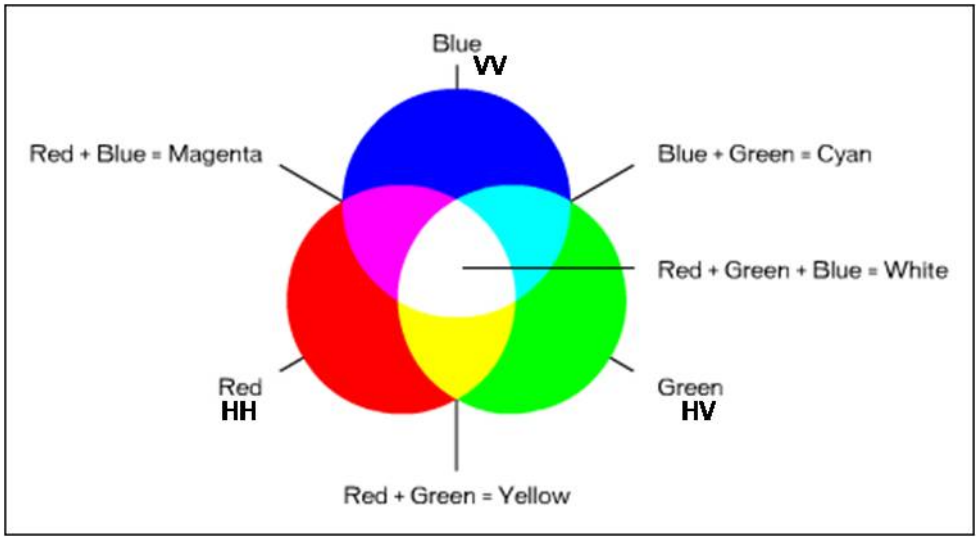

Figure 2.4: Color wheel for interpreting of the interaction between the RGB colors and polarization channels.

2.3 Color Spaces and Synthetic Aperture Radar (SAR) Multicolor Imaging.

Multicolor SAR imagery can be created by encoding three different combinations of transmitter and receiver polarization with any tristimulus color space (also known as color model). This can be done by assigning each of the three color components to a particular polarization channel. Using the RGB color space as an example, we can use the following basic color-polarization code which the linear decomposition model, which is the basic decomposition technique and considers to map a color vector with a polarization channel as described in Table 2.1:

Table 2.1: Color code for different combinations of polarizations.

Polarization	Color
VV	green
HH	red
HV	blue

When the three channels are combined equally, that means that each channel has the same value in a particular pixel, the resulting color will be a shade of gray. Otherwise,

the color displayed will point to the dominant (or subordinate) channel or channels. By watching the colors of the generated image, we can make some interpretation of the scatterers present in the scene. For example, the absence of Red appears Cyan, the absence of Green appears Magenta, the absence of Blue appears Yellow. By using this relationship we can say a relatively strong HH scatterer will appear Red while a relatively weak HH scattering will appear Cyan.

2.3.1 Colorimetry. According to [31], Colorimetry is a discipline of color science that is mainly concerned with numerically describing the color of a physically defined visual stimulus in a way that:

- the image it is been viewed by an observer with normal color vision;
- under same observing conditions;
- stimuli with the same specification look alike;
- stimuli that look alike have same specification;
- the quantities describing these specifications are continuous function of the physical parameters defining the spectral radiant power distribution of the stimulus.

This definition set a big number of conditions in order to determine or perform any comparison between the same imagery with different color spaces. When we talk about color technology, there are some facts that need to be considered. Today, color technology is a very broad science that is growing and improving on a day by day basis due to the technology and available high power computation. This facts lead to a very dynamic field that is developed according to the objective for which it is being adapted. The color space depends directly on the electronic color-device to be used [12]. The color spaces used for this research were RGB as used in the television industry and computer monitors and CMY as used in the printer industry.
These device-dependent color spaces were created for convenience of use, digital representation and computation and are independent of the way that the observer can sense this stimulus as a color format. This means that in the way that the informa-

tion is intended to be delivered will depend directly in the capacity of the observer to process that stimulus information through their own sensors, which, for the human case are the eyes [12, 18, 30, 31].

Light is located in a narrow range of the electromagnetic waves and the frequencies or wavelength are detectable by the human eye. Color describes a particular characteristic of an object facilitating and simplifying object identification and extraction of information from a scene. We must consider also that humans can discern thousands of color shades and intensities, which is very relevant when the image analysis is performed by humans.

Within the electromagnetic spectrum of the light, different perceptions of colors can be produced, for example a long wavelength produce the perception of red, while a short wavelength produce the perception of violet. The process of color sensing is produced by the physical stimulation of light detectors known as cones, in the human retina [12,18]. The spectrum of colors produced by a prism is referred to as spectrally pure or monochromatic and each of these colors are related to a particular wavelength. This means that when we talk about a spectrally pure color, we are referring to a single wavelength, but that can be produced by a combination of colors. For example, an orange color is associated with a wavelength of $\lambda = 600\ nm$. The same color can be produced with a combination of two light beams, one being red with a wavelength of $\lambda = 700\ nm$, and another being yellow with a wavelength of $\lambda = 580\ nm$, with no orange component [12, 18, 30, 31].

Color image processing is divided into two major areas [6, 18, 30]: full color and pseudocolor processing. In the first case, the images are acquired with a full-color sensor, such as color camera or color scanner. In the second case, a color is assigned to a particular monochrome intensity or range of intensities. For example, colored images of polarimetric SAR systems, where each channel or different combinations of polarimetric channels represent the intensity values for a given color. In order to distinguish one color from another, three characteristics are used. These characteristics are *brightness*, *hue* and *saturation* [6,18,31]. Brightness maps the achromatic notion

of intensity. Hue is an attribute associated with the dominant wavelength in a mixture of light waves. Hue represents a dominant color as perceived by an observer. Thus, when we call an object red, orange or yellow, we are referring to its hue. Saturation refers to the relative purity or the amount of white light mixed with a hue.

The combination of Hue and saturation is known as *chromacity* [6, 31], and therefore, a color may be characterized by its brightness and chromacity. The amounts of red, green and blue needed to form any particular color are known as *tristimulus* [6,18,30,31] values and are denoted, X, Y, and Z, respectively. A color is then defined by its *trichromacity* coefficients, defined as [6, 18, 30, 31]:

$$x = \frac{X}{X + Y + Z} \tag{2.20}$$

$$y = \frac{Y}{X + Y + Z} \tag{2.21}$$

$$z = \frac{Z}{X + Y + Z} \tag{2.22}$$

It is noted from these equations that

$$x + y + z = 1 \tag{2.23}$$

2.3.2 Color Image Processing on SAR Imagery. What we obtain after raw data from a SAR system is processed is a graphical representation of the relation between the strength of the signal received from a point scatter and the location of that point scatter within the scene. For a fully polarimetric SAR system, four channels with different scatter response from the same point scatter are collected. In order to form a SAR image, the contribution of each polarization channel is of interest for the observer, due to in this way, more features are revealed on the image. By assigning a particular color to each polarization channel, we can identify its contribution for a particular pixel, making it even easier for an analyst to identify a particular feature or target of interest [16, 19, 22].

2.3.2.1 Color Spaces. The purpose of a color space (also color space or color system) is to facilitate the specification of colors in some standard, generally accepted way. In essence, a color model is a specification of a coordinate system and a subspace within that system where each color is represented by a single point.
Most color models in use today are oriented either toward hardware (such as for color monitors and printers) or toward applications where color manipulation is a goal (such as in the creation of color graphics for animation) [6, 18]. In terms of digital image processing, the hardware-oriented models most commonly used in practice are the *RGB* (red, green, blue) model for color monitors and a broad class of color video cameras and *CMY* (cyan, magenta, yellow) and *CMYK* (cyan, magenta, yellow, black) model for color printing [6].

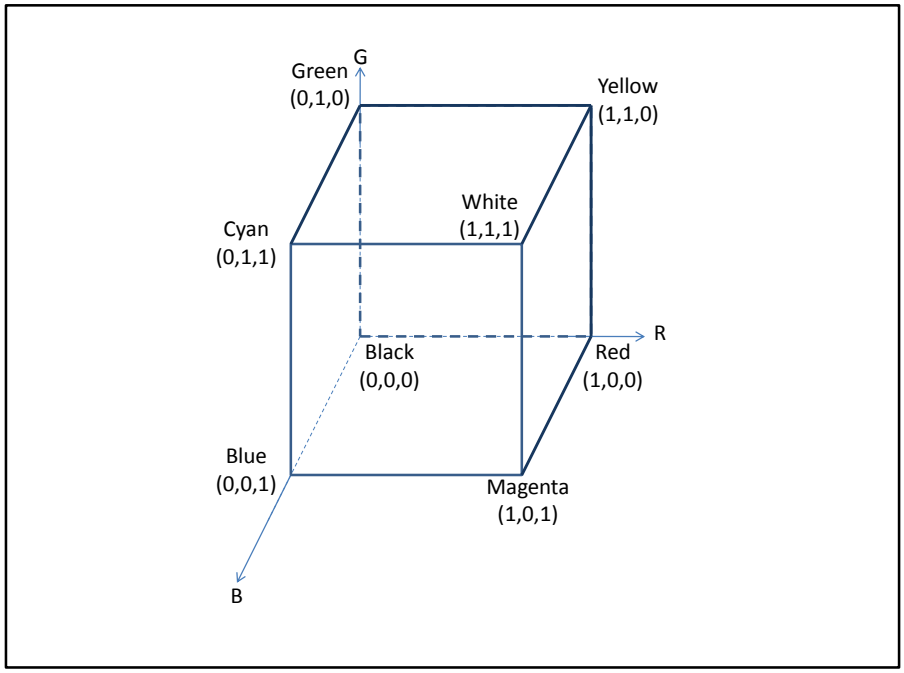

Figure 2.5: The RGB cube representing the RGB color space with all color components as a vector form [12].

2.3.2.2 RGB (Red Green Blue) Color Space. The RGB (Red, Green, Blue) color model is very well known and widely used. This color space is defined in terms of three vectors identified as Red, Green, and Blue which each having domain

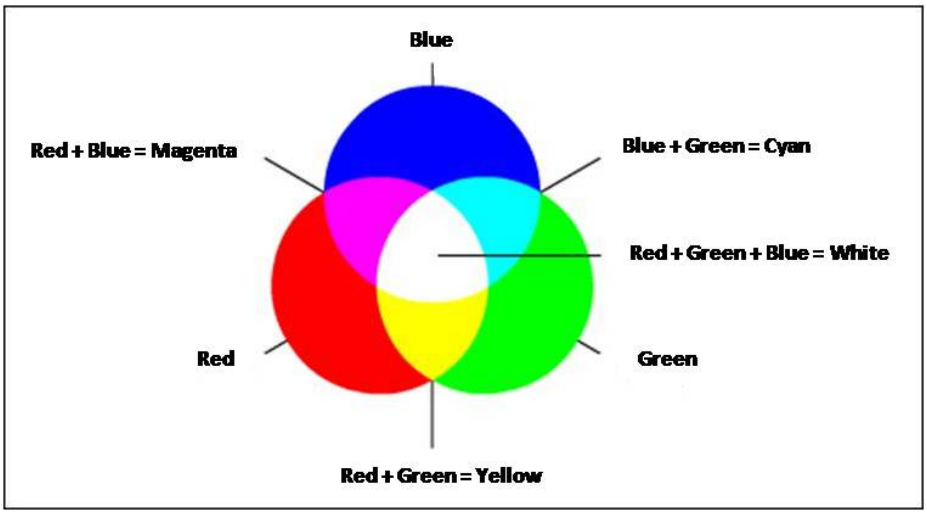

Figure 2.6: A graphic representation of the RGB color space is presented. The three fundamental colors Red, Blue and Green are shown as well as the result of the addition between them.

values of $[0 - 255]$: A tri-color mixture is considered additive because other colors are formed by combining the primary colors: Red, Green and Blue. When the three colors are combined with the highest value, the result is white. When the three colors are combined with the lowest value, the color is black [7, 12, 33]. Figure 2.6 shows RGB primary colors and their combinations.

2.3.2.3 CMY (Cyan Magenta Yellow) Color Space. The CMY, is another well known color space, widely used in the color printing industry. This color space is based in the secondary colors of light cyan, magenta, and yellow or primary colors of pigments [6,12]. These are each represented as vectors with domain values of $[0\% - 100\%]$: Different colors can be created by superimposing three images; one for cyan, one for magenta and one for yellow. The CMY color space is really a combination of primary colors (Cyan, Magenta, Yellow) as a result of subtracting the RGB color space from white light. The three components represent three reflection filters that create an optical illusion based on light absorption [7, 29]. Figure 2.8 shows CMY primary colors and their combinations. For example, when a surface coated with cyan pigment is illuminated with white light, no red light is reflected

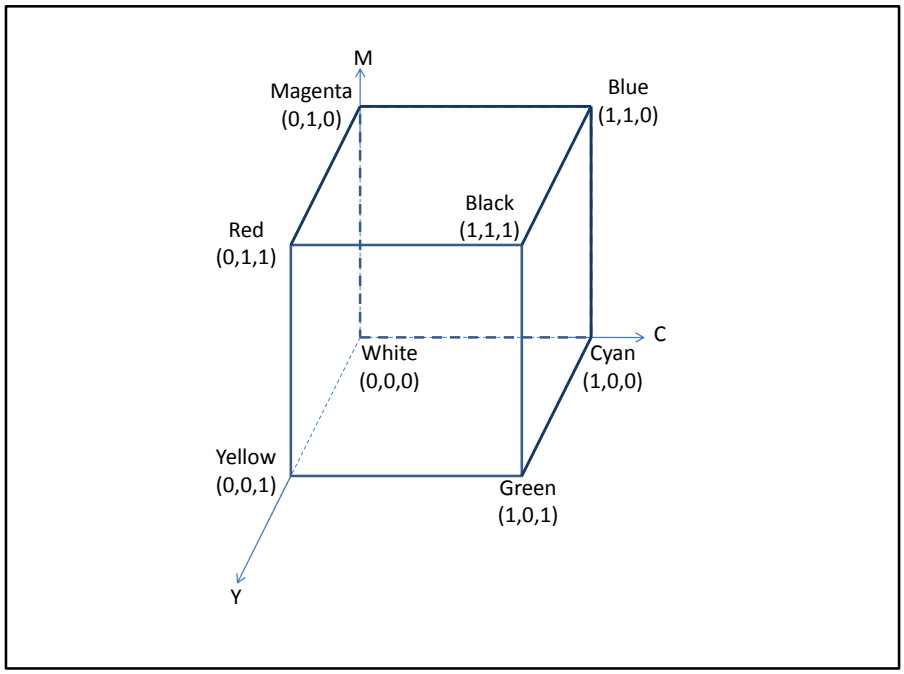

Figure 2.7: The CMY cube representing the CMY color space with all color components as a vector form [12].

from the surface. That is, cyan subtracts red light from reflected white light, which itself is composed of equal amounts of red, green, and blue light.

Most devices that deposit colored pigments on paper, such as color printers and copiers, require CMY data input or perform an RGB to CMY conversion internally [12]. This conversion is performed using the simple operation

$$\begin{bmatrix} C \\ M \\ Y \end{bmatrix} = \begin{bmatrix} 1 \\ 1 \\ 1 \end{bmatrix} - \begin{bmatrix} R \\ G \\ B \end{bmatrix} \tag{2.24}$$

Equation (2.24) demonstrates that light reflected from a surface coated with pure cyan does not contain red (that is, $C = 1 - R$ in the equation). Ideally, cyan, magenta and yellow are sufficient to generate a wide range of colors by the subtractive process, but if we mix the same quantity of the three colors, we should get black, but in practice, a dark brown is generated. For this reason, a fourth real black ink is

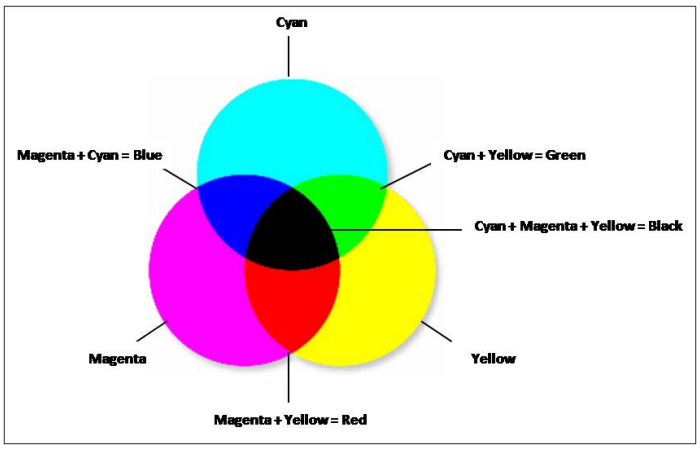

Figure 2.8: A graphic representation of the CMY color space. The three fundamental colors: Cyan, Magenta and Yellow are shown as well as the result of the interaction between them.

added in printing process to obtain true color, what is known as $CYMK$ color space. Similarly, pure magenta does not reflect green, and pure yellow does not reflect blue. Equation (2.24) also reveals that RGB values can be obtained easily from a set of CMY values by subtracting the individual CMY values from 1. As indicated earlier, in image processing, this color model is used in connection with generating hard copy output, so the inverse operation from CMY to RGB generally is of little practical interest.

2.4 Polarimetric Systems

Over the years, the development of space and airborne SAR systems for the observation of the earth has experienced a rapid growth. A variety of SAR systems, airborne and spaceborne, have provided researchers with high quality SAR data from different locations and points of interest, providing multiple frequency and polarization observations for both military and civilian analysis [16, 19].

The ENVISAT satellite, developed by European Space Agency (ESA), was launched on March 2002, and was the first civilian satellite with dual-polarization advanced synthetic aperture radar (ASAR) system operating in C-band. The first fully PolSAR

satellite was the Advance land Observing Satellite (ALOS), a Earth-observation satellite developed by the Japan Aerospace Exploration Agency (JAXA), Japan launched in January 2006. This satellite includes an L-band polarimetric radar sensor (PALSAR) used for environmental and hazard monitoring. TerraSAR-X developed by the German Aerospace Center (DLR), EADS-Astrium and Infoterra GmbH was launched in 2007 and carries a dual-polarimetric and high frequency X-band sensor and can be operated in a quad-pol mode. Another polarimetric spaceborne sensor is RADARSAT-2, developed by the Canadian Space Agency (CSA) and MacDonald, Dettwiler and Associates Ltd. Industries (MDA), lunched successfully in December 2007 and was designed to monitoring Canada's icy waterways [16].

Now, we will describe some airborne polarimetric SAR systems. The AIRSAR was designed and built by the Jet Propulsion Laboratory (NASA-JPL) in the early 80's. This L-band radar was flown on a NASA Ames Research Center CV-990 Airborne Laboratory. After an accident of this airborne platform, an upgraded radar polarimeter was built at JPL and was known as AIRSAR, operated in the fully polarimetric modes at P-band(0.45 GHZ), L-band(1.26 GHZ), and C-band(5.31 Ghz) bands simultaneously. AIRSAR also considered an along-track interferometer (ATI) and cross-track interferometric (XTI) modes in L-band and C-band, respectively. AIRSAW first flew in 1987 and conduct at least one flight campaign each year in US and international missions also.

The Convair-580 C/X SAR system is an airborne SAR developed by the Canada Centre for Remote Sensing (CCRS) since 1974. The Convair-580 C/X SAR system is a dual-frequency polarimetric SAR operating at C-band (5.30 GHz) and X-band (9.25 GHz). The primary mission of this SAR system is remote sensing research, including developments of applications of RADARSAT data [16].

The EMISAR is a C-band(5.3 GHz), vertically polarized, airborne SAR . It was developed by the Technical University of Denmark (TUD), Electromagnetics Institute (EMI) in 1989. In 1995, it was upgraded to a fully polarimetric capability and is flown in a Gulfstream G3 aircraft of the Royal Danish Air Force. The primary mission of

this SAR system is data acquisition for the research of the Danish Center for Remote Sensing (DCRS).

There are several other polarimetric spaceborne and airborne SAR systems gathering data for military and civilian purposes. For this reason, research on this area is a necessity in order to process data and get high quality information from SAR imagery [16, 19, 22].

III. Decomposition Techniques on SAR Polarimetry and Colorimetry applied to SAR Imagery.

Several developments have been made including methods like Van Zyl's [14] which decompose S in three types of dominant scattering mechanisms. This method, which is similar to Freeman's decomposition, is applicable for distributed targets such as ocean and forested surfaces because Van Zyl's and Freeman's methods were used primarily to denote the difference between rough flat surfaces such as the ocean, volume scatterers such as forest, and dihedral corner reflections such as man-made objects or natural features such as the intersection of a tree trunk and the ground. As presented in [26], the SAR community has been developing different techniques in order to determine SAR signatures based upon characterization and statistical analysis of measured data. This signature is highly dependent on the season, environmental conditions and events. Much of the SAR polarimetric related research has been focused on establishing an optimal orientation in order to maximize the signal-to-noise ratio. In the case of the "Gotcha Volumetric SAR Data Set, Version 1.0" release [4], 2-D and 3-D imaging of stationary targets from wideband, fully polarimetric data is investigated. The SAR system operated in the circular mode and completed 8 circular orbits around the scene at incremented altitudes. The distributed data included phase history data, auxiliary data, processed images, ground truth pictures and a collection summary report making it an ideal set to investigate the scattering matrix decomposition and multi-color processing. For this research, a sparse data is analyzed using Pauli and Krogager decomposition techniques, combined with RGB and CMY color spaces in order to determine the best combination of decomposition technique and color space for feature extraction. In order to obtain a quantitative metric of performance, the CRLB is established for comparing the different permutations [25]. The two decomposition techniques are presented in the following section.

3.1 Decomposition techniques on SAR Polarimetry.

According to [16, 19, 22], SAR polarimetry provides data about the polarization state of the returned electromagnetic energy (radar signal) for every resolution element or pixel, which complements the intensity information contained in the scattering matrix of the target return. Therefore, the author used SAR polarimetry to produce a scattering matrix by transmitting two orthogonally polarized waves in which we have called horizontal and vertical polarization. Each radar echo is also received on two orthogonally polarized antennas giving a fully polarimetric set of data (HH, HV, VV, VH). By correlating the signals in range and azimuth, the author measured the relative phase differences of the received voltages and coherently add all returns to construct a SAR image [16, 17]. Ultimately, information about the environment is obtained through the study of the reflectivity function which reveals how the electromagnetic waves interacted with the environment [16]. The generic equation for the scattering matrix S is

$$S = \sum_{k=1}^{N} \alpha_k S_k \tag{3.1}$$

where α_k is a complex weight for a particular scattering mechanism represented by its scattering matrix S_k. Fully polarimetric systems normally provide four channels described by the scattering matrix [22]:

$$S_k = \begin{bmatrix} S_{hh} & S_{vh} \\ S_{hv} & S_{vv} \end{bmatrix} \tag{3.2}$$

where the term S_{xy} represents the scattering vector due to x-polarization upon transmit and y-polarization upon receive. Reciprocity of the cross-channels is normally assumed, meaning $S_{hv} = S_{vh}$ [16, 19, 22]. Due to this characteristic, the matrix S can be represented by three channels, S_{hh}, S_{vv}, S_{vh} or S_{hv}.

The images in Figure 3.1 through Figure 3.8 were obtained from the "Gotcha Volumetric SAR Data Set, Version 1.0". Reciprocuty of polarization channels S_{hv} S_{vh} is assumed, because both channels have practically the same contribution as

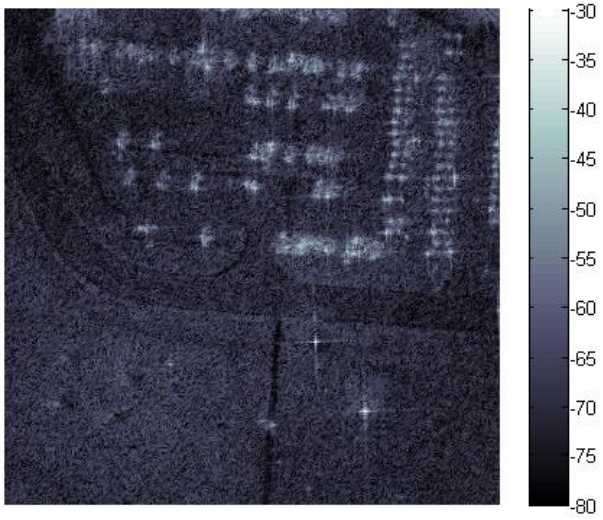

Figure 3.1: SAR image from sparse "Gotcha Volumetric SAR Data Set, Version 1.0" (one pass, one collection) for VV Polarization. This image was obtained by using a polar format algorithm and has no further processing.

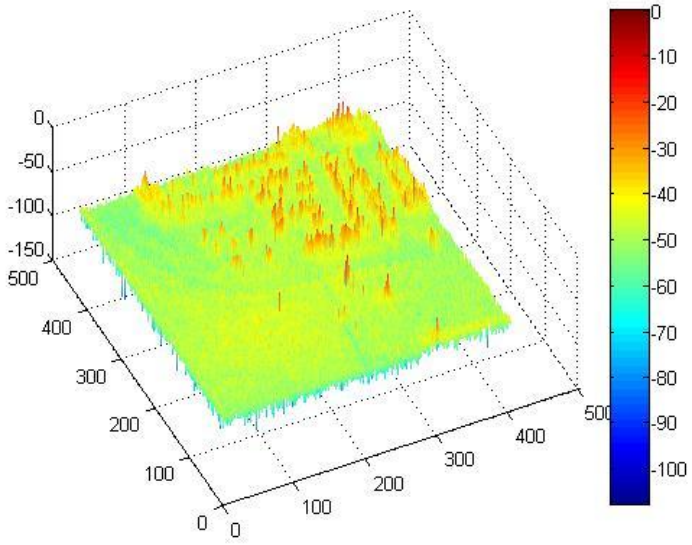

Figure 3.2: Representation of the energy scattered for each pixel of the SAR image can be observed. This surface plot was obtained from sparse "Gotcha Volumetric SAR Data Set, Version 1.0" (one pass, one collection) for VV polarization channel and is the same data set used to obtain the SAR image in figure 3.1.

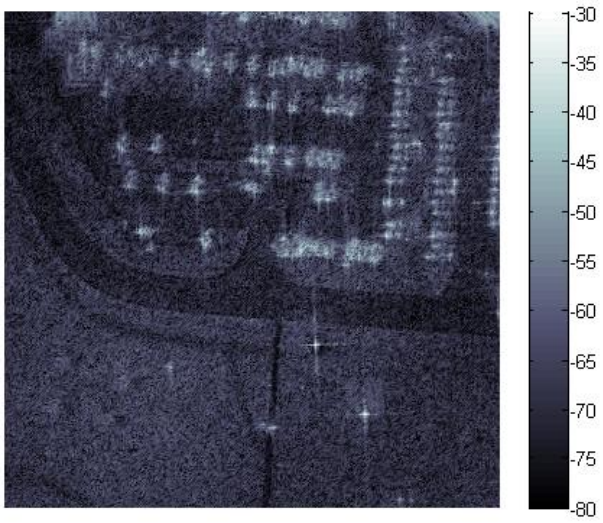

Figure 3.3: SAR image from sparse "Gotcha Volumetric SAR Data Set, Version 1.0" (one pass, one collection) for HH Polarization. This image was obtained by using a polar format algorithm and has no further processing.

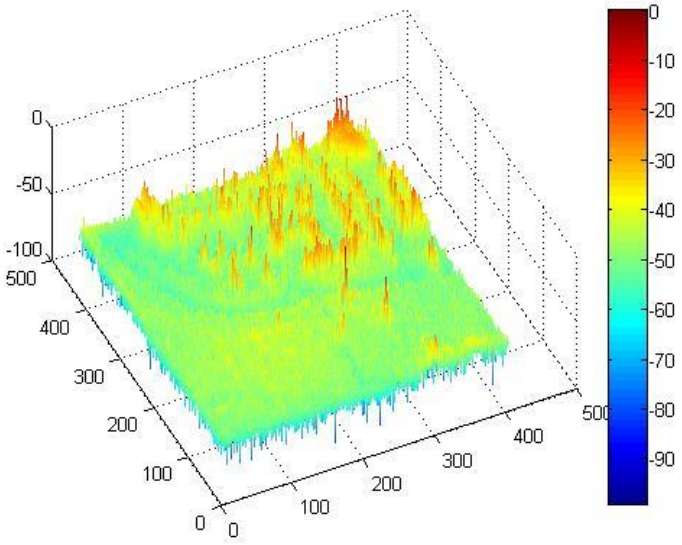

Figure 3.4: Representation of the energy scattered for each pixel of the SAR image can be observed. This surface plot was obtained from sparse "Gotcha Volumetric SAR Data Set, Version 1.0" (one pass, one collection) for HH polarization channel and is the same data set used to obtain the SAR image in figure 3.3.

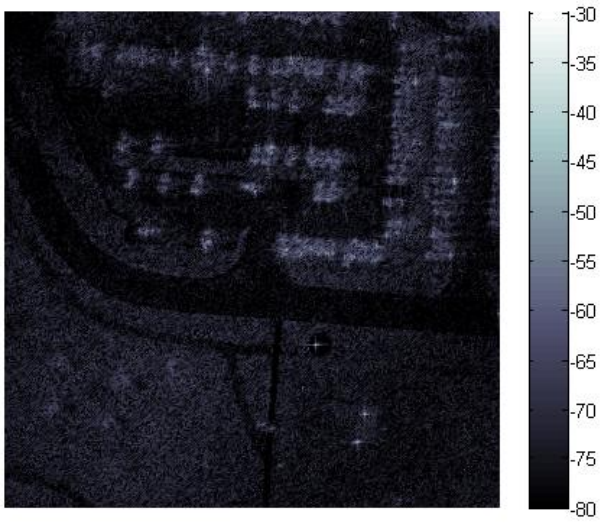

Figure 3.5: SAR images from sparse "Gotcha Volumetric SAR Data Set, Version 1.0" (one pass, one collection) for VH Polarization. This images where obtained by using a polar format algorithm and has no further processing.

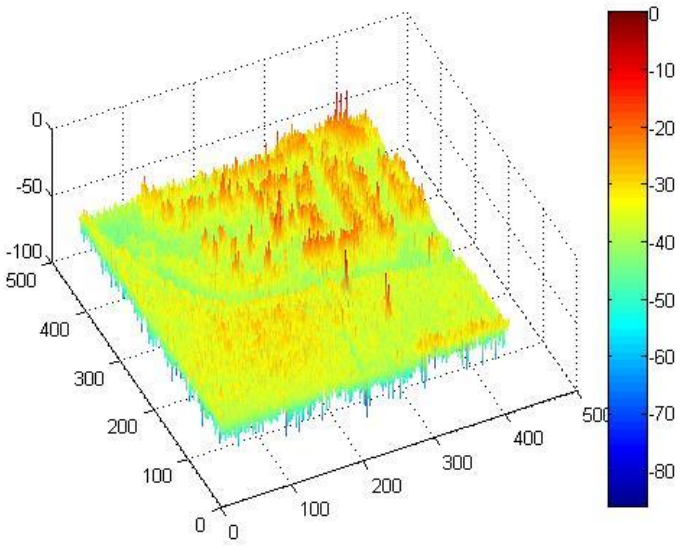

Figure 3.6: Representation of the energy scattered for each pixel of the SAR image can be observed. This surface plot was obtained from sparse "Gotcha Volumetric SAR Data Set, Version 1.0" (one pass, one collection) for VH polarization channel and is the same data set used to obtain the SAR image in figure 3.5.

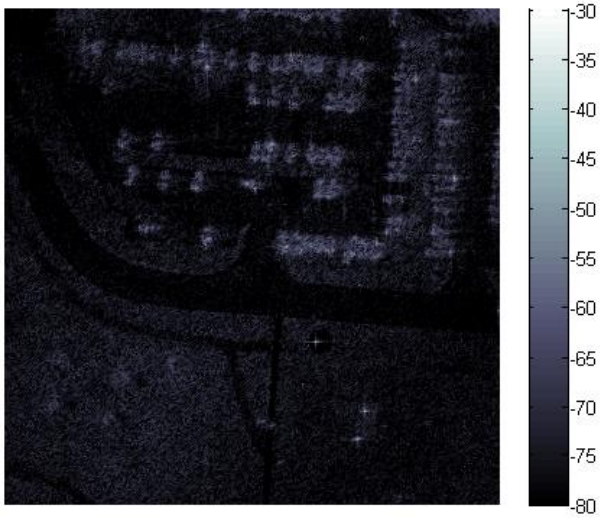

Figure 3.7: SAR images from sparse "Gotcha Volumetric SAR Data Set, Version 1.0" (one pass, one collection) for HV Polarization. This images where obtained by using a polar format algorithm and has no further processing.

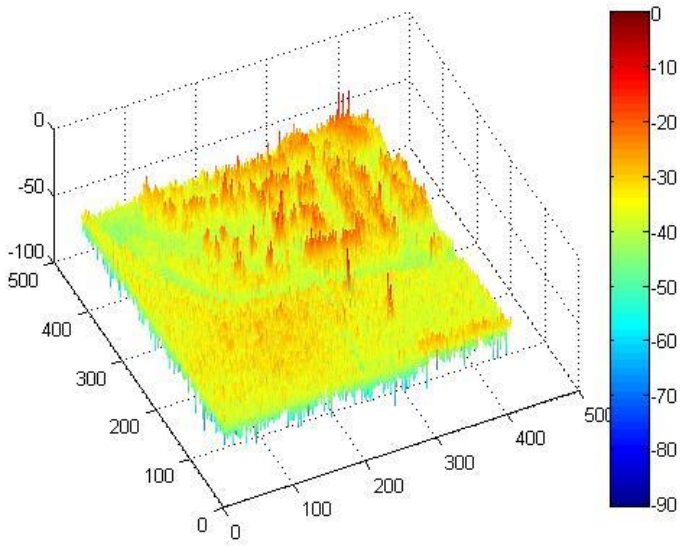

Figure 3.8: Representation of the energy scattered for each pixel of the SAR image can be observed. This surface plot was obtained from sparse "Gotcha Volumetric SAR Data Set, Version 1.0" (one pass, one collection) for HV polarization channel and is the same data set used to obtain the SAR image in figure 3.7.

observed on figures 3.5 through 3.8. As seen in equations (3.1) and (3.2), scattering matrix is a linear combination of basis matrices corresponding to canonical scattering mechanisms. For simplicity, the scattering matrix is treated as the characterization of a single coherent scatter at each pixel. For this research, no external disturbances due to background clutter or to time fluctuation of the target are assumed. In the following, three common approaches to coherent decomposition (Pauli and Krogager) are discussed.

3.1.1 Linear Decomposition. The linear decomposition is the basic decomposition technique, because it just considers the very same information obtained from each polarization channel, without further processing. Under this scheme, the information obtained from each channel will correspond directly to a vertical to vertical, horizontal to horizontal or cross-polarized scatter.

The linear decomposition is defined as follows:

$$\overline{k}_l = \begin{bmatrix} k_1 \\ k_2 \\ k_3 \end{bmatrix} = \begin{bmatrix} S_{hh} \\ \sqrt{2}S_{hv} \\ S_{vv} \end{bmatrix} \tag{3.3}$$

and it can be color-coded as indicated in Table 3.1

Table 3.1: Color code for linear decomposition.

Vector	Mechanism	Color
k_1	S_{hh}	red
k_2	$\sqrt{2}S_{vh}$	green
k_3	S_{vv}	blue

3.1.2 Pauli Decomposition. This decomposition uses Pauli matrices, for the basis expansion of S_k as:

$$S_k = \begin{bmatrix} S_{hh} & S_{hv} \\ S_{vh} & S_{vv} \end{bmatrix}$$

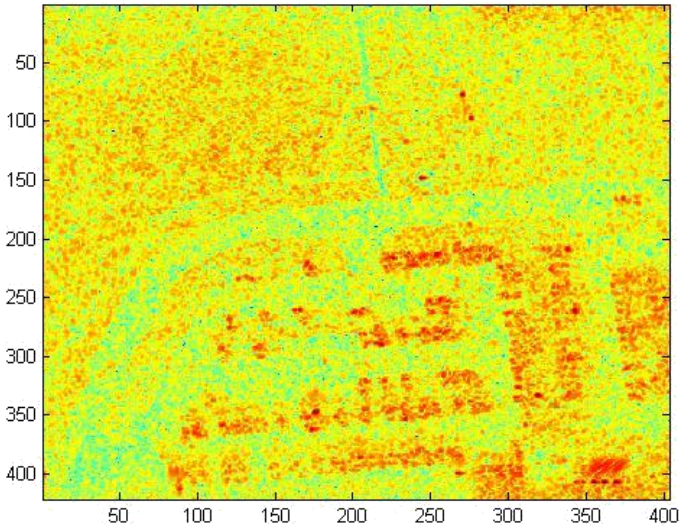

Figure 3.9: A representation of the energy present for the k_1 component (S_{hh}) at each pixel can be observed. The k_1 component corresponds to a scatter of a horizontal oriented target scattering. For this SAR image, the presence of objects present in the scene that reflect the energy transmitted in horizontal polarization without changing polarization state are highlighted.

$$= \frac{a}{\sqrt{2}} \begin{bmatrix} 1 & 0 \\ 0 & 1 \end{bmatrix} + \frac{b}{\sqrt{2}} \begin{bmatrix} 1 & 0 \\ 0 & -1 \end{bmatrix} + \frac{c}{\sqrt{2}} \begin{bmatrix} 0 & 1 \\ 1 & 0 \end{bmatrix} + \frac{d}{\sqrt{2}} \begin{bmatrix} 0 & -j \\ j & 0 \end{bmatrix} \tag{3.4}$$

and a, b, c and d are all complex values and are given by

$$a = \frac{S_{hh} + S_{vv}}{\sqrt{2}} \tag{3.5}$$

$$b = \frac{S_{hh} - S_{vv}}{\sqrt{2}} \tag{3.6}$$

$$c = \frac{S_{hv} + S_{vh}}{\sqrt{2}} \tag{3.7}$$

$$d = j\frac{S_{hv} - S_{vh}}{\sqrt{2}} \tag{3.8}$$

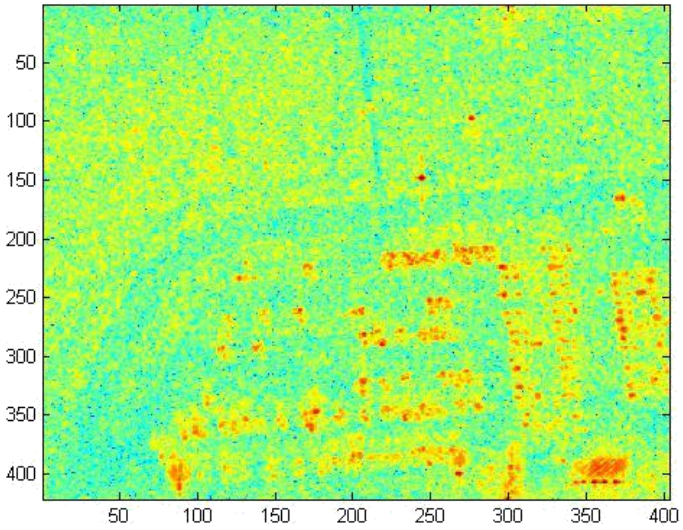

Figure 3.10: A representation of the energy present for the k_2 component (S_{vh} or S_{hv}) at each pixel can be observed. The k_2 component corresponds to a cross-polarized scatter. For this SAR image, the presence of objects present in the scene that backscatter by changing polarization state are highlighted.

The application of the Pauli decomposition to deterministic targets may be considered the coherent composition of four scattering mechanisms: the first being single scattering from a plane surface (single or odd-bounce scattering), the second and third being diplane scattering (double or even-bounce scattering) from corners with a relative orientation of 0° and 45°, respectively, and the final element being all the antisymmetric components of the scattering S matrix [16,22,24,28]. These interpretations are based on consideration of the properties of the Pauli matrices when they undergo a change of wave polarization basis. In the monostatic case, where $S_{hv} = S_{vh}$, the Pauli matrix basis can be modified in its c and d terms as shown on equations (3.9) and (3.10):

$$c = \frac{S_{hv} + S_{vh}}{\sqrt{2}} = 2\frac{S_{hv} + S_{hv}}{\sqrt{2}} = 2\frac{S_{vh} + S_{vh}}{\sqrt{2}} = 2\frac{S_{hv}}{\sqrt{2}} = 2\frac{S_{vh}}{\sqrt{2}} \tag{3.9}$$

$$d = j\frac{S_{hv} - S_{vh}}{\sqrt{2}} = j\frac{S_{hv} - S_{hv}}{\sqrt{2}} = j\frac{S_{vh} - S_{vh}}{\sqrt{2}} = j\frac{0}{\sqrt{2}} = 0 \tag{3.10}$$

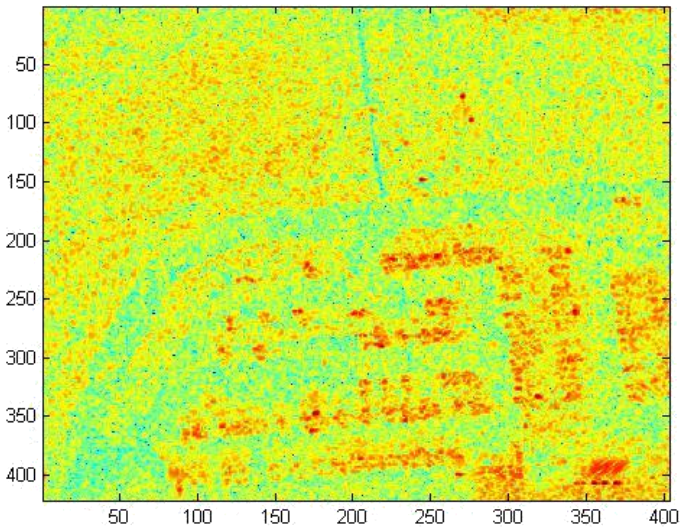

Figure 3.11: A representation of the energy present for the k_3 component (S_{vv}) at each pixel can be observed. The k_3 component corresponds to a scatter of a vertical oriented target scattering. For this SAR image, the presence of objects present in the scene that reflect the energy transmitted in vertical polarization without changing polarization state are highlighted.

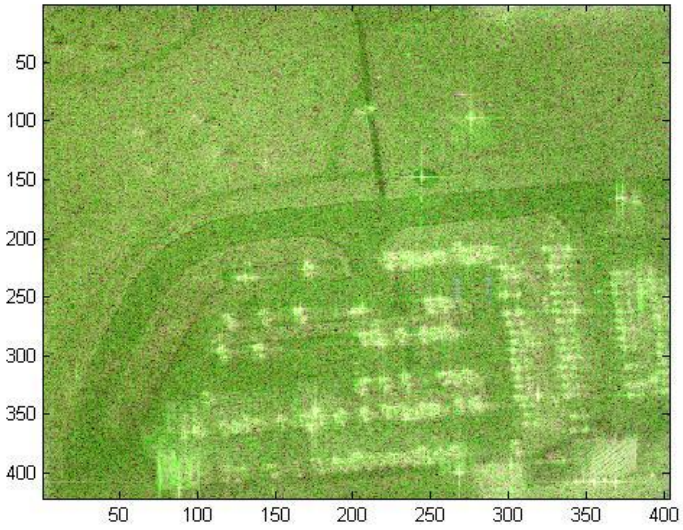

Figure 3.12: SAR images using Linear decomposition from sparse "Gotcha Volumetric SAR Data Set, Version 1.0" (one pass, one collection). This SAR image combine the contribution of the three previous images in terms of energy present for each image pixel.

The final expression for the Pauli matrix basis, is described as a coherent scattering vector $\overline{k}_P$ as follows:

$$\overline{k}_P = \begin{bmatrix} k_1 \\ k_2 \\ k_3 \end{bmatrix} = \frac{1}{\sqrt{2}} \begin{bmatrix} S_{hh} + S_{vv} \\ 2S_{hv} \\ S_{vv} - S_{hh} \end{bmatrix} \tag{3.11}$$

Figure 3.16 describes the result of the Pauli decomposition on a SAR image from the "Gotcha Volumetric SAR Data Set, Version 1.0". The color was coded using RGB color space as shown on Table 3.2. The k_1 component corresponds to a scatter of a sphere, a plate or a trihedral and is referred to a single-bounce or odd-bounce scattering. The k_2 component corresponds to the scattering mechanism of a diplane oriented at 45 degrees. This last component is referred to a target that returns a wave with polarization orthogonal to the incident wave, hence we can say that this component represent volumetric scatters like the one produced by the forest canopy. The k_3 component represents the scattering mechanism of a dihedral oriented a 0 degrees and is referred to a double-bounce or even-bounce [16, 19, 22].

Table 3.2: Color code for Pauli decomposition.

Vector	Mechanism	Color
k_1	$\frac{1}{\sqrt{2}}(S_{hh} + S_{vv})$	red
k_2	$\frac{1}{\sqrt{2}}(2S_{hv})$	green
k_3	$\frac{1}{\sqrt{2}}(S_{vv} - S_{hh})$	blue

3.1.3 Krogager Decomposition. In this case, a scattering matrix is decomposed into three coherent components which are interpreted as scattering from a sphere, diplane, and helix targets under a change of rotation angle θ, as follows in the scattering matrix in the linear polarization basis $S_{(H,V)}$ [16, 19, 22, 24, 28]:

$$S_{(H,V)} = e^{j\phi} \left\{ e^{j\phi_S} k_S S_{\text{sphere}} + k_D S_{\text{diplane}_{(\theta)}} + k_H S_{\text{helix}_{(\theta)}} \right\} \tag{3.12}$$

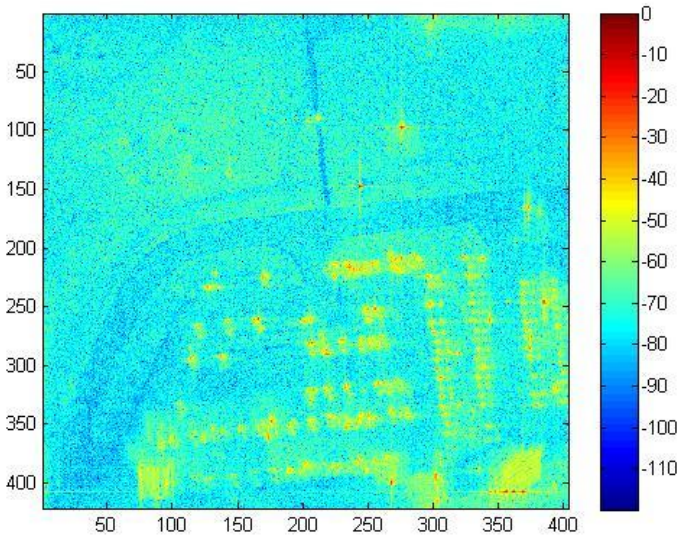

Figure 3.13: Representation of the energy present for the k_1 component $(S_{hh} + S_{vv})$ at each pixel can be observed. The k_1 component corresponds to a scatter of a sphere, a plate or a trihedral and is referred to a single-bounce or odd-bounce scattering. For this SAR image, the presence of man-made kind of objects present in the scene are highlighted in the sense that the energy is strong for these structures.

$$S_{\text{sphere}} = \begin{bmatrix} 1 & 0 \\ 0 & 1 \end{bmatrix} \tag{3.13}$$

$$S_{\text{diplane}_{(\theta)}} = \begin{bmatrix} \cos 2\theta & \sin 2\theta \\ \sin 2\theta & -\cos 2\theta \end{bmatrix} \tag{3.14}$$

$$S_{\text{helix}_{(\theta)}} = e^{\mp j2\theta} \begin{bmatrix} 1 & \pm j \\ \pm j & -1 \end{bmatrix} \tag{3.15}$$

where k_S, k_D and k_H correspond to the sphere, diplane, and helix contribution; θ is the orientation angle and ϕ is the absolute phase.

The phase ϕ_S represents the displacement of the sphere relative to the diplane inside the resolution cell. This circular polarization basis $S_{(R,L)}$ is related to the linear polarization basis $S_{(H,V)}$ by the following equations [10, 14, 32]:

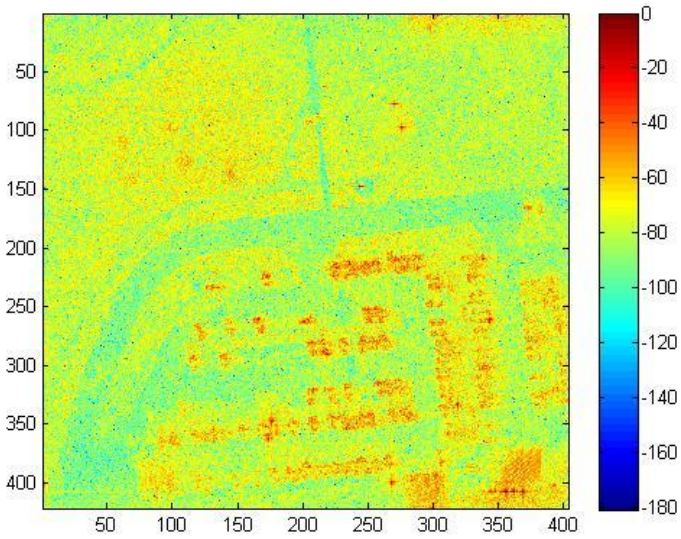

Figure 3.14: Representation of the energy present for the k_2 component ($2S_{hv}$) at each pixel can be observed. The k_2 component corresponds to the scattering mechanism of a diplane oriented at 45 degrees. This last component is referred to a target that returns a wave with polarization orthogonal to the incident wave, hence we can say that this component represent volumetric scatters like the one produced by the forest canopy. For this SAR image, volumetric scatter is evidenced in the scene.

$$S_{rr} = jS_{hv} + \frac{1}{2}(S_{hh} - S_{vv}) \tag{3.16}$$

$$S_{ll} = jS_{hv} - \frac{1}{2}(S_{hh} - S_{vv}) \tag{3.17}$$

$$S_{rl} = S_{lr} = \frac{1}{2}(S_{hh} + S_{vv}) \tag{3.18}$$

Expressed in terms of the circular polarization basis $S_{(R,L)}$, the Krogager decomposition is now given by

$$S_{(R,L)} = \begin{bmatrix} S_{rr} & S_{rl} \\ S_{lr} & S_{ll} \end{bmatrix}$$

$$= e^{j\phi}\left(e^{j\phi_S}k_S\begin{bmatrix} 0 & j \\ j & 0 \end{bmatrix}t + k_D\begin{bmatrix} e^{j2\theta} & 0 \\ 0 & -e^{-j2\theta} \end{bmatrix} + k_H\begin{bmatrix} e^{j2\theta} & 0 \\ 0 & 0 \end{bmatrix}\right) \tag{3.19}$$

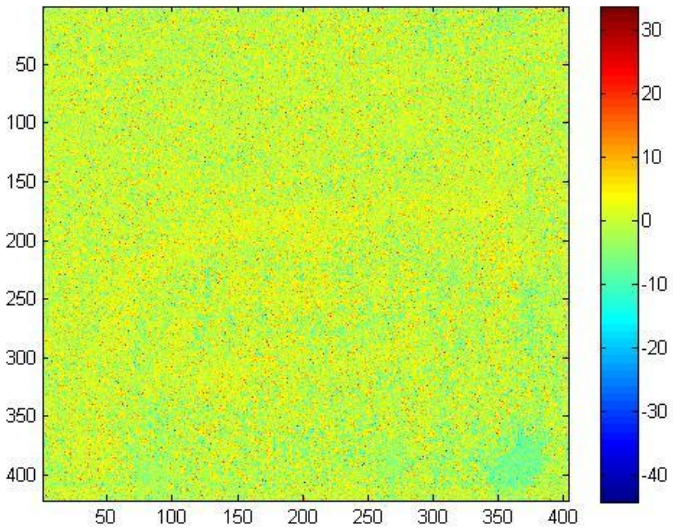

Figure 3.15: Representation of the energy present for the k_3 component $(S_{vv} - S_{hh})$ at each pixel can be observed. The k_3 component represents the scattering mechanism of a dihedral oriented a 0 degrees and is referred to a double-bounce or even-bounce. For this SAR image, the lack of features that can provide double or even bounce is observed.

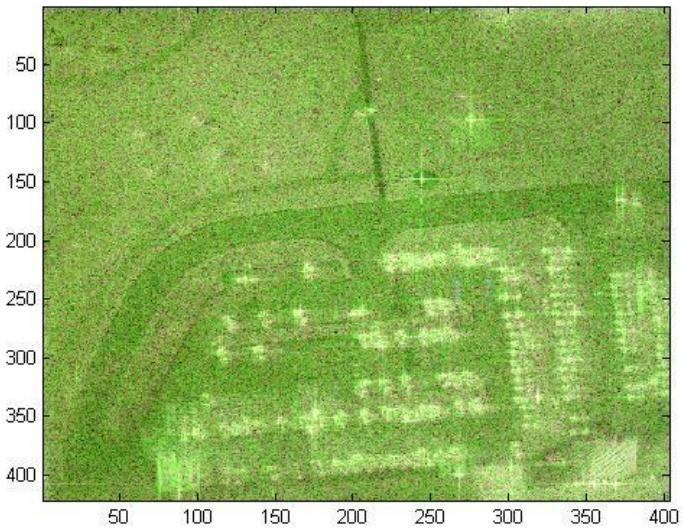

Figure 3.16: SAR images using Pauli decomposition from sparse "Gotcha Volumetric SAR Data Set, Version 1.0" (one pass, one collection). This SAR image combine the contribution of the three previous images in terms of energy present for each image pixel.

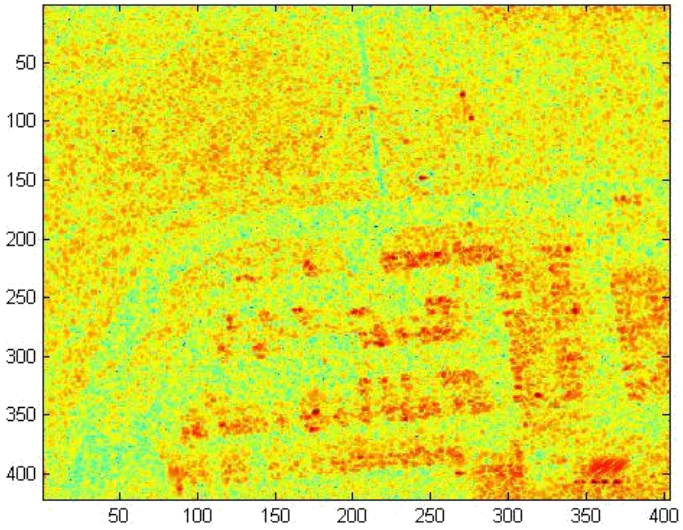

Figure 3.17: Representation of the energy present for the k1 component ($jS_{hv} + \frac{1}{2}(S_{hh} - S_{vv})$) at each image pixel can be observed.

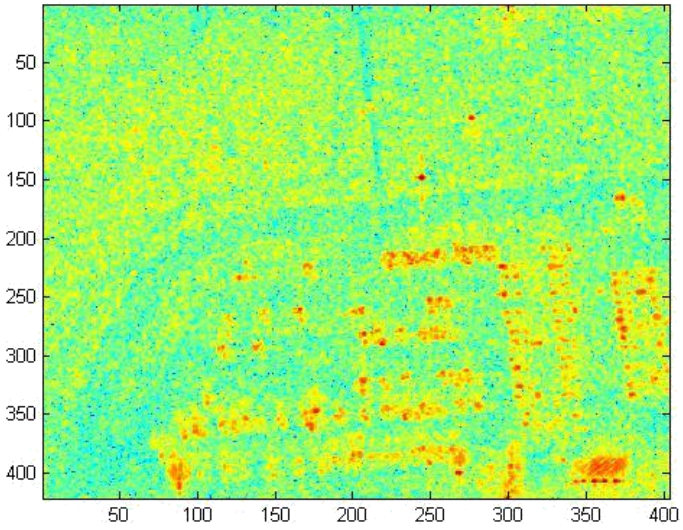

Figure 3.18: Representation of the energy present for the k2 component ($\frac{1}{2}(S_{hh} + S_{vv})$) at each image pixel can be observed.

The elements S_{rr} and S_{ll} directly represent the diplane component. Due to this condition, two cases of analysis must be made according to whether $|S_{rr}|$ is greater or less than $|S_{ll}|$:

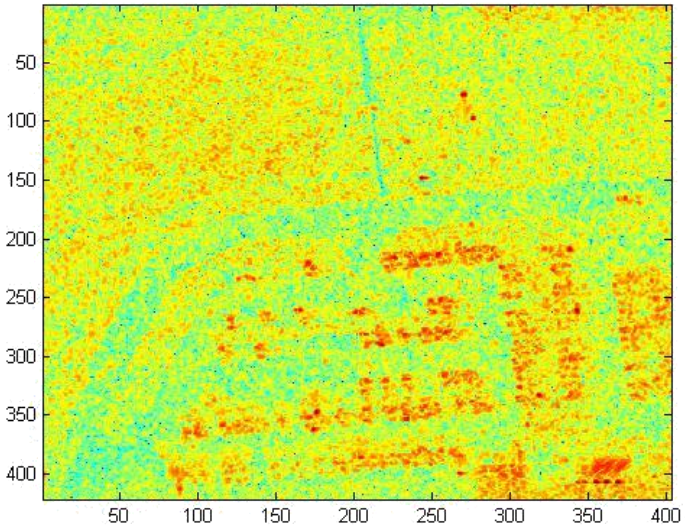

Figure 3.19: Representation of the energy present for the k3 component ($jS_{hv} - \frac{1}{2}(S_{hh} - S_{vv})$) at each image pixel can be observed.

$$|S_{rr}| \geq |S_{ll}| \Rightarrow \begin{cases} \overset{k_D^+ = |S_{ll}|}{k_H^+ = |S_{rr}| - |S_{ll}|} \Leftarrow \text{Left sense helix} \end{cases}$$

$$|S_{rr}| \leq |S_{ll}| \Rightarrow \begin{cases} \overset{k_D^- = |S_{rr}|}{k_H^- = |S_{ll}| - |S_{rr}|} \Leftarrow \text{Right sense helix} \end{cases}$$

It is also important to note that the three Krogager decomposition parameters (k_S, k_D, k_H) are parameters independent of orientation, in other words, roll-invariant parameters. This roll-invariant characteristic give a more stable characterization of a target of interest.

The final expression for the Krogager matrix basis, is described as a coherent scattering vector $\overline{k}_C$ as follows:

$$\overline{k}_C = \begin{bmatrix} k_1 \\ k_2 \\ k_3 \end{bmatrix} = \frac{1}{\sqrt{2}} \begin{bmatrix} jS_{hv} + \frac{1}{2}(S_{hh} - S_{vv}) \\ \frac{1}{2}(S_{hh} + S_{vv}) \\ jS_{hv} - \frac{1}{2}(S_{hh} - S_{vv}) \end{bmatrix} \tag{3.20}$$

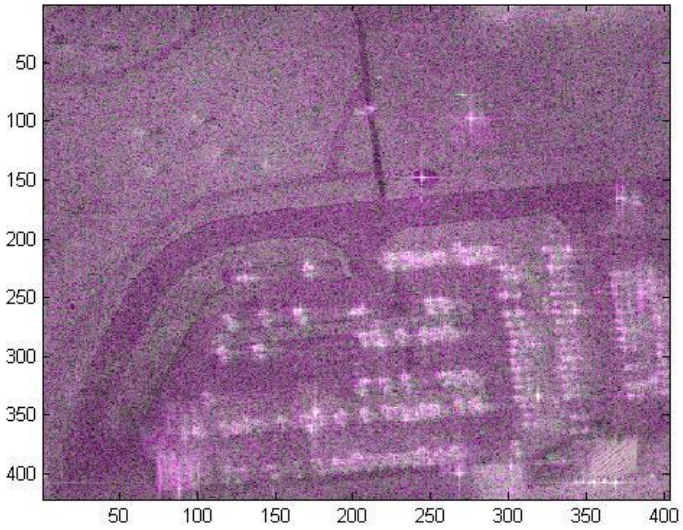

Figure 3.20: SAR images using Krogager decomposition from sparse "Gotcha Volumetric SAR Data Set, Version 1.0" (one pass, one collection).

Finally, the Krogager decomposition can be color-coded as shown on Table II:

Table 3.3: Color code for Krogager Decomposition.

Vector	Mechanism	Color
k_1	$jS_{hv} + \frac{1}{2}(S_{hh} - S_{vv})$	red
k_2	$\frac{1}{2}(S_{hh} + S_{vv})$	green
k_3	$jS_{hv} - \frac{1}{2}(S_{hh} - S_{vv})$	blue

3.1.4 Crámer-Rao Lower Bound. With today's technology and scientific development, tools to estimate or predict the performance of unknown parameters from a set of measurements is a task that can save a lot of time, and effort. Crámer-Rao Lower Bound (CRLB) is useful to calculate lower bounds to the variances of any estimate of a set of parameters (also known as unbiased CRLB). With this technique, we can determine, a priori, whether or not a desired estimation accuracy can be achieved for a given measurement model. Using probability density function (PDF) of the measurements as a function of the true parameter values, bounds can be calculated.

An unbiased parameter estimate is not always possible or desirable (excessive noise amplification in the unbiased parameters) [20].

The Crámer-Rao Lower Bound will be used as a metric of comparison between combination of both, decomposition methods and color spaces. In the parameter estimate problems of signals embedded in noise, the bias and the variance of the estimate error are particularly significant in evaluating the estimator performance. The CRLB will tell us how difficult it is to estimate a parameter based in a particular data model [3, 8, 11, 21]. The CRLB bound of the error correlation matrix $\mathbf{E}\left[\left(\widehat{\Phi}-\Phi\right)\left(\widehat{\Phi}-\Phi\right)^{T}\right]$ is given by [8, 25]:

$$\mathbf{MSE}\left(\Phi\right) \geq \frac{\partial \mathbf{E}\left[\widehat{\phi}\right]}{\partial \Phi}\mathbf{J}^{-1}\left(\Phi\right)\frac{\partial \mathbf{E}\left[\widehat{\phi}\right]}{\partial \Phi}^{T} + \left(\mathbf{E}\left[\widehat{\Phi}\right]-\Phi\right)\left(\mathbf{E}\left[\widehat{\Phi}\right]-\Phi\right)^{T} \tag{3.21}$$

where the matrix $\mathbf{J}\left(\Phi\right)$ is referred to as the Fisher Information Matrix (FIM), and $\mathbf{E}\left[\widehat{\Phi}\right]-\Phi$ represents the bias estimator. The $\mathbf{MSE}\left(\Phi\right)$ is the error correlation matrix since the diagonal terms of $\mathbf{E}\left[\left(\widehat{\Phi}-\Phi\right)\left(\widehat{\Phi}-\Phi\right)^{T}\right]$ represent the **MSE**. where $\widehat{\Phi}$ represents our vector of unknown parameters and Φ represents our vector of known parameters.

Considering that the purpose of this research is to give a quantitative reason of why one decomposition technique is more efficient than the other one in the sense that will be more easy for an operator to extract the important feature of a target present on a particular scene, the author propose to use the CRLB as a measure of performance of how well a set of data can be estimated.

If the aim is to estimate one or a set of parameters Φ, an estimator $\widehat{\Phi}(y_1, y_2, ..., y_N)$ must be created. This estimator is a function of the N observations $y(t_1), y(t_1), ..., y(t_N)$. The N observations are random variables, making the estimator a random variable as well. The mean and the variance of $\widehat{\Phi}$ gives a measure of how good an estimate of the estimator $\widehat{\Phi}$ is. For this research, the known parameter Φ for each decomposition

technique is described as follows:

$$\Phi_{linear} = \begin{bmatrix} A_1 \\ A_2 \\ A_3 \end{bmatrix}_{linear} = \begin{bmatrix} S_{hh} \\ \sqrt{2}S_{hv} \\ S_{vv} \end{bmatrix} \tag{3.22}$$

$$\Phi_{pauli} = \begin{bmatrix} A_1 \\ A_2 \\ A_3 \end{bmatrix}_{pauli} = \frac{1}{\sqrt{2}} \begin{bmatrix} S_{hh} + S_{vv} \\ 2S_{hv} \\ S_{vv} - S_{hh} \end{bmatrix} \tag{3.23}$$

$$\Phi_{Krogager} = \begin{bmatrix} A_1 \\ A_2 \\ A_3 \end{bmatrix}_{Krogager} = \frac{1}{2} \begin{bmatrix} S_{hh} - S_{vv} + 2iS_{hv} \\ S_{hh} + S_{vv} \\ S_{hh} - S_{vv} - 2iS_{hv} \end{bmatrix} \tag{3.24}$$

and the estimators for each decomposition are in the form described as follows

$$\widehat{\Phi}_{linear} = \begin{bmatrix} \widehat{A}_1 \\ \widehat{A}_2 \\ \widehat{A}_3 \end{bmatrix}_{linear} \tag{3.25}$$

$$\widehat{\Phi}_{pauli} = \begin{bmatrix} \widehat{A}_1 \\ \widehat{A}_2 \\ \widehat{A}_3 \end{bmatrix}_{pauli} \tag{3.26}$$

$$\widehat{\Phi}_{Krogager} = \begin{bmatrix} \widehat{A}_1 \\ \widehat{A}_2 \\ \widehat{A}_3 \end{bmatrix}_{Krogager} \tag{3.27}$$

Since we are trying to estimate a vector of parameters which correspond to the three components for each decomposition, the estimator is described as follows

$$\Phi = [A_1, A_2, A_3]^T \tag{3.28}$$

where $A1$, $A2$, $A3$, corresponds to the complex value of each image pixel of the three decomposition components at which a color vector will be assigned.
The best situation is when the estimator is unbiased, at the same time that is desirable for the variance of the estimator $\mathbf{E}(\widehat{\Phi} - \Phi)^2$ to be as small as possible. This method will establish a lower bound on the variance of any estimator, setting a limit on the accuracy that can be achieved.

The CRLB for an estimation of a parameter vector is

$$J^{-1}([A_1, A_2, A_3]) \tag{3.29}$$

where Equation 3.29 is the Fisher Information Matrix (FIM). The diagonal of this matrix contains the CRLB for each parameter. The FIM contains the derivatives with respect to the components of the parameter vector of the log-likelihood, l for the probability density function.

IV. Performance Limits for Colored SAR Imagery and feature Extraction

4.1 Data Set Description.

The data set used for this research is the "Gotcha Volumetric SAR Data Set, Version 1.0". The data set was publicly released by the Air Force Research Laboratory as a Challenge Problem to the SAR community interested in 2D/3D imaging of stationary targets. The data set was produced by a fully polarimetric SAR system mounted in an airborne platform and has a center frequency of 9.6 GHz with a bandwidth of 640 MHz. The data consists of eight circular passes at a different elevation angles, collecting data at each angle of the 360^o for every pass. The data is in a Matlab format (*.mat files) and each file contains the phase history collected for each azimuth angle of each pass considering the four different polarization.

The MATLAB data structure contains the k-space data, frequencies, range to the scene center, x, y, z coordinate antenna locations, elevation and azimuth angle in degrees. The target area is a parking lot with different models of passenger car, a case tractor, a forklift and different calibration targets such a large top hat reflector, dihedral and trihedral reflectors [1, 5].

4.2 Processing Raw SAR Data for Image Formation.

The algorithm used to generate the data and images from the Gotcha data set for a scattering matrix decomposition analysis were obtained using an algorithm on MATLAB programming software.

4.2.1 Polarimetric Image Formation. The Gotcha data set was collected by flying around the target in circles. Under this scenario, the data processing and the algorithm were developed considering a spotlight mode SAR. For this research, the Polar Format Algorithm (PFA) was used to transform the raw data, which is in the spatial frequency (k-space) domain, to an (spatial image) domain. This is, the information of complex values of amplitude and phase in the k-space is transformed

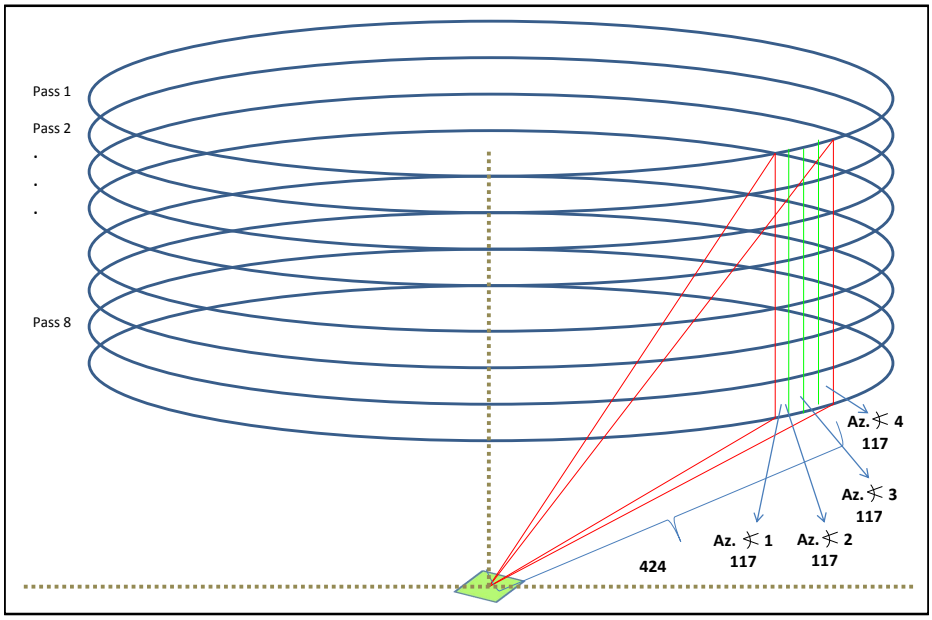

Figure 4.1: The Gotcha data set contains 8 passes at different altitudes. Each pass considers 360^o for the four polarization channels. Each azimuth angle contains frequency history with the detail of range cells and pulses.

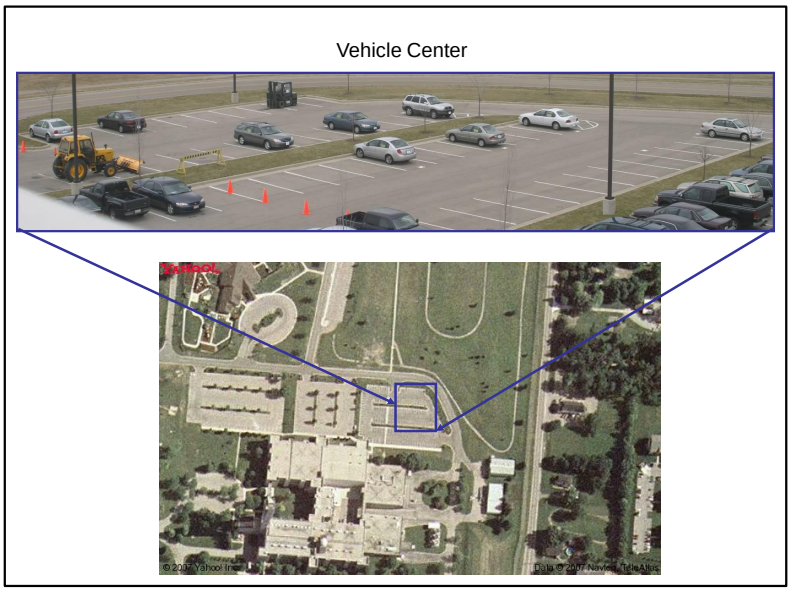

Figure 4.2: Target area for Gotcha data collection. Different types of passenger cars can be observed as well as a forklift and a case tractor. Calibration targets are not shown in this photo. (Photo from Gotcha data set documentation released by AFRL.) [1].

into an intensity value for each pixel on the resulting image [11,22] as shown on Figure 4.4.

4.2.1.1 Polar Format Algorithm (PFA). The PFA map the samples in the frequency domain to the spatial frequency domain. In the reconstruction process, the samples in spatial domain are interpolated from its available polar samples by using two one-dimensional interpolation by each dimension in order to obtain the data in a rectangular format. Once in a rectangular format, a two-dimensional windowing process is used to get rid of the side lobes influence. Finally, a Inverse Fourier Trasform is performed to obtain our complex image as shown on Figure 4.3 [11, 19, 28].

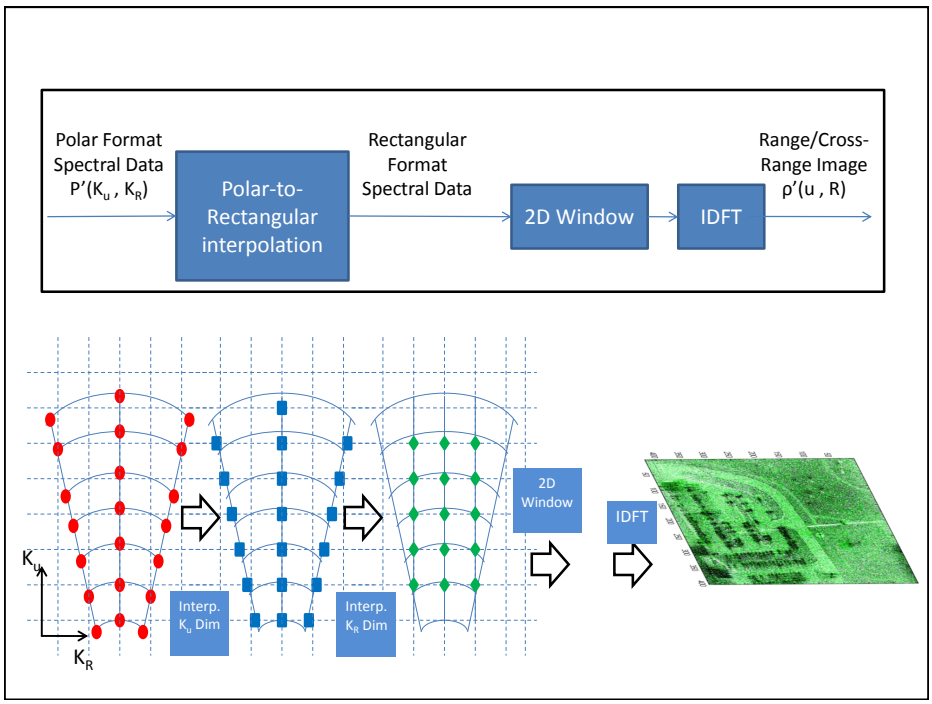

Figure 4.3: Block Diagram of PFA process [24].

4.2.1.2 Data Processing for Polarimetric Analysis. Once the data is in the image domain, an image can be formed by using the data from each polarization channel. At this point, the intensity information for each image pixel is available. Due to the random nature and the different shapes present in the target, the characteristics of the return are different for each polarization channel. For this reason, the data

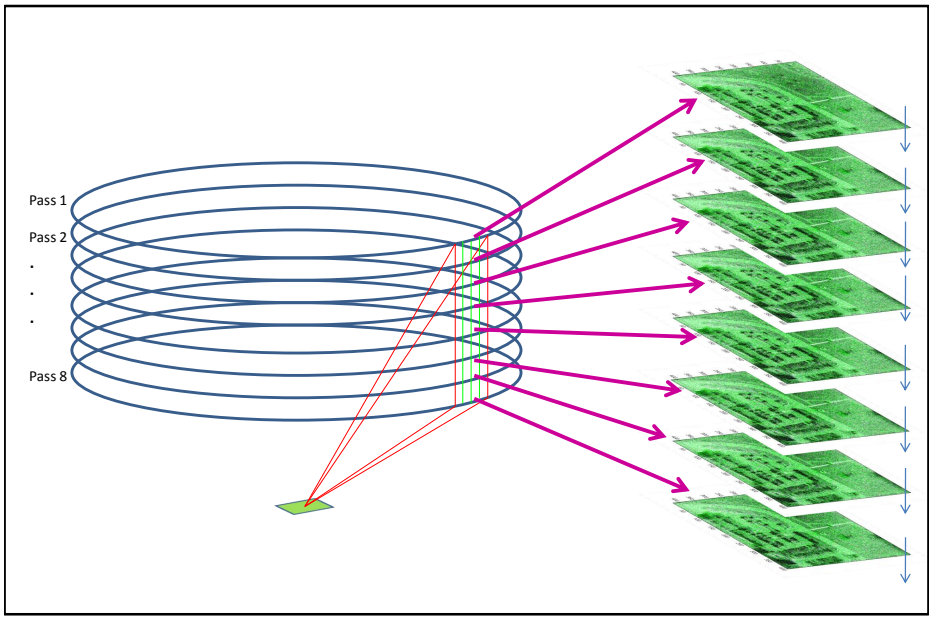

Figure 4.4: Graphic description of the process of computing a SAR image from raw Gotcha data. The eight passes are shown, as well as the imagery that can be obtained from each azimuth angle and polarization channel.

must be scaled and normalized. In order to scale the data, a Dynamic Range (DR) process is used. This process is performed by extracting the mean value considering the maximum and minimum amplitude value, considering the data from the three polarization channels. The mean value will be used as the central value of the DR and the data considered for each polarimetric channel is the data within the range plus and minus half the value of the total DR from this mean value. By using this process, the contribution from each polarization channel is assured. At this point we have an image for each polarization channel with information of intensity for each image pixel. Once we have the data scaled and normalized for each decomposition channel, we use the different decomposition techniques, as described in chapter III to build our image in a format of tristimulus values for each pixel. This means that each image pixel had the contribution of three different intensity values, one for each layer as shown on Figure 4.5. These values are obtained from the mathematical relationship between channels that are dictated for each decomposition technique as

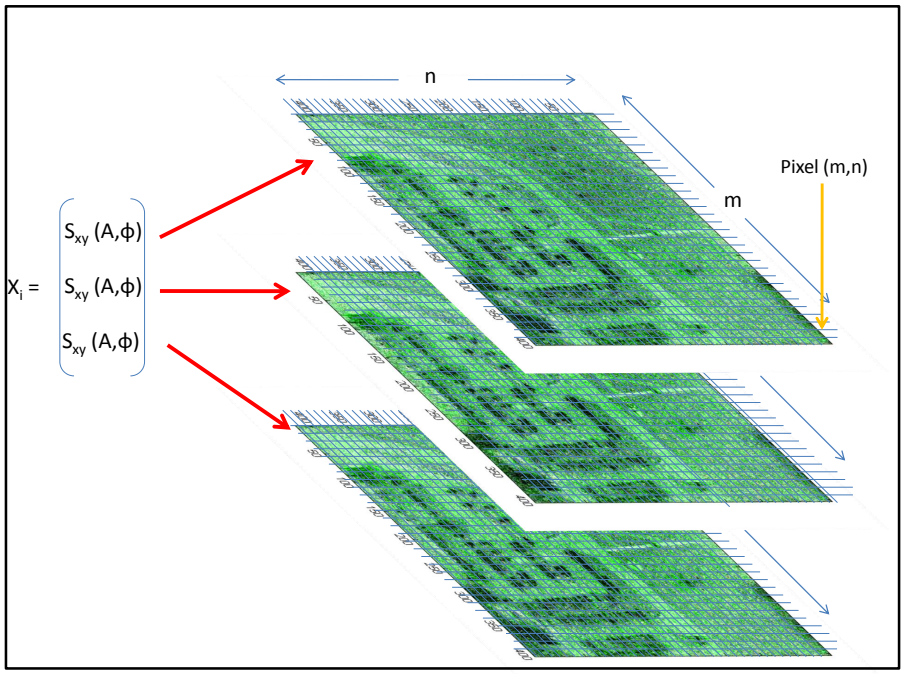

Figure 4.5: Graphic description of a decomposed SAR image by the three components of a particular decomposition technique represented by the vector X_i.

was described in chapter III. A color vector is assigned for each layer of the resulting colored SAR image. For the case of RGB Color Space, the red color vector is assigned to the first layer, Green is assigned to the second layer and Blue is assigned to the third layer [23]. In the case of the (m^{th}, n^{th}) pixel, this will combine the intensity contribution displaying a color which will be the resulting combined color from the three intensity values.

4.2.2 SAR imagery Obtained from Gotcha Data Set. By using the data set described in section 4.1 and the algorithm described in section 4.2. Several sets of images using all eight passes were computed. These images consider two color spaces, RGB and CMY and the results are shown on the set of images from Figure 4.6 to Figure 4.29. Further comments on these figures are made at the end of this section.

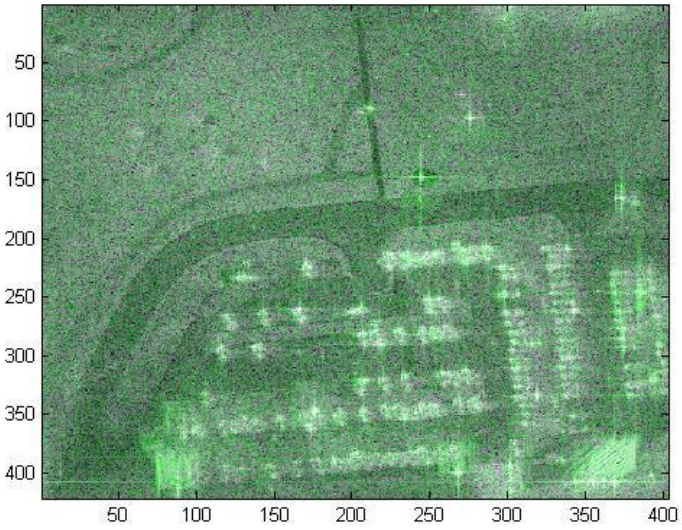

Figure 4.6: This is a SAR image using linear decomposition, obtained computing the SAR raw data from pass1, azimuth angle number one and RGB color space.

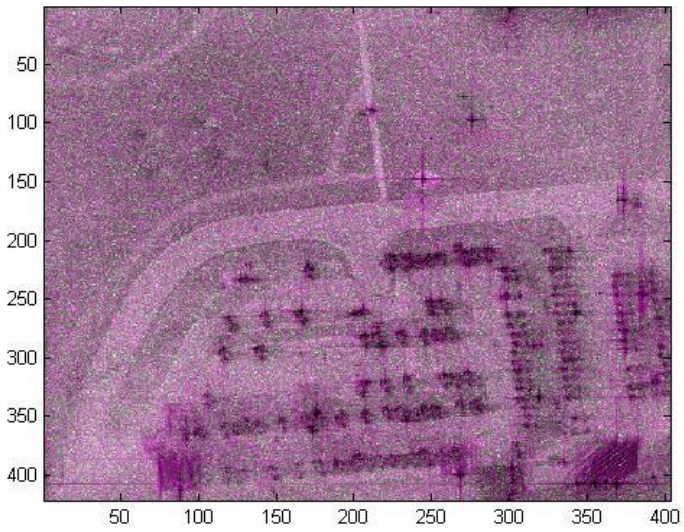

Figure 4.7: This is the same SAR image on Figure 4.6 but computed for CMY color space. The process of compute the CMY color space image is by subtracting the RGB values of Figure 4.6 from one.

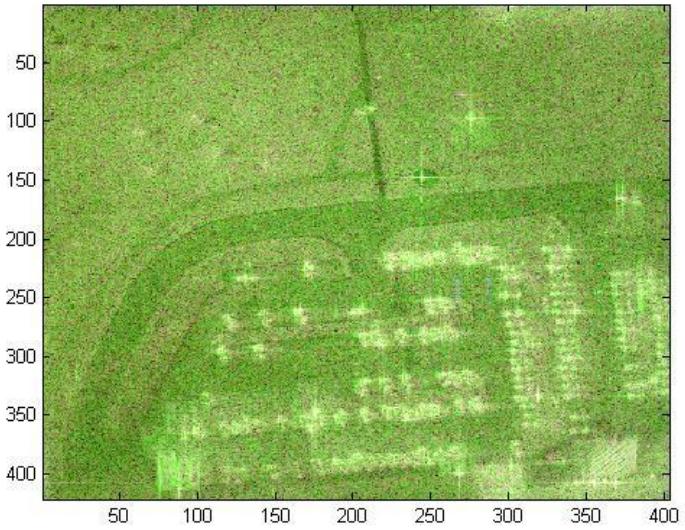

Figure 4.8: This is a SAR image using Pauli decomposition, obtained computing the SAR raw data from pass1, azimuth angle number one and RGB color space.

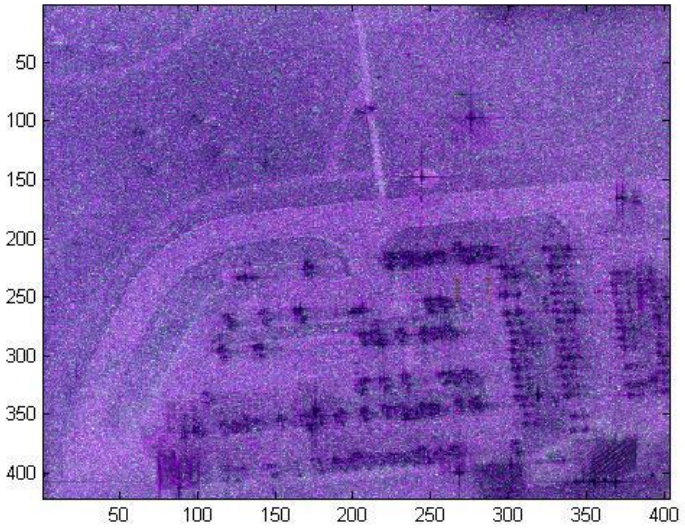

Figure 4.9: This is the same SAR image on Figure 4.8 but computed for CMY color space. The process of compute the CMY color space image is by subtracting the RGB values of Figure 4.8 from one.

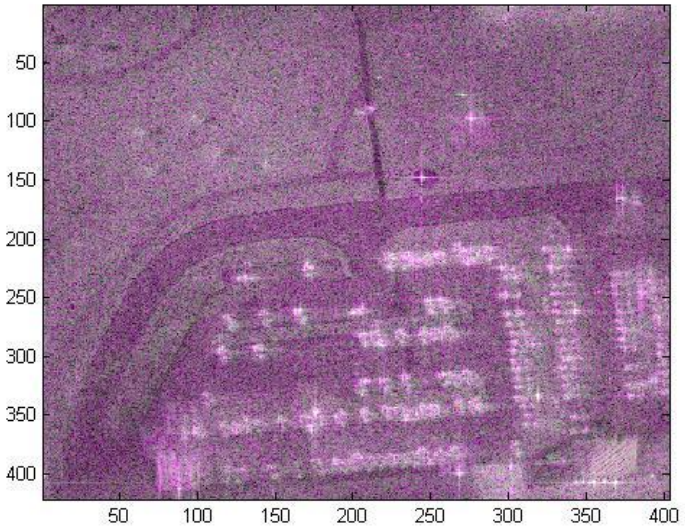

Figure 4.10: This is a SAR image using Krogager decomposition, obtained computing the SAR raw data from pass1, azimuth angle number one and RGB color space.

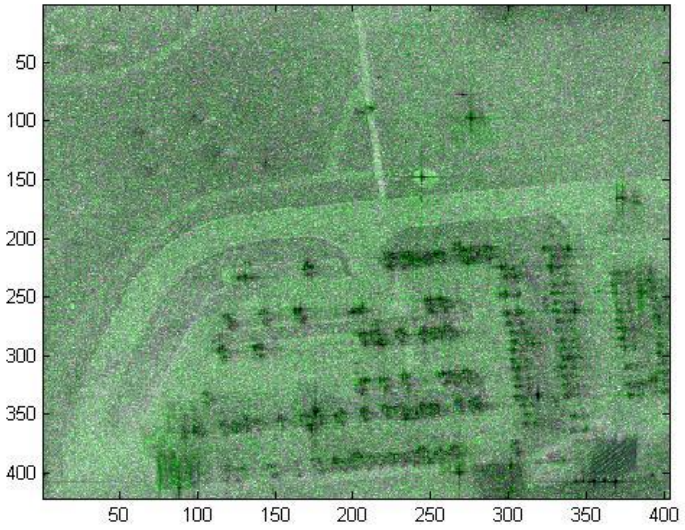

Figure 4.11: This is the same SAR image on Figure 4.10 but computed for CMY color space. The process of compute the CMY color space image is by subtracting the RGB values of Figure 4.10 from one.

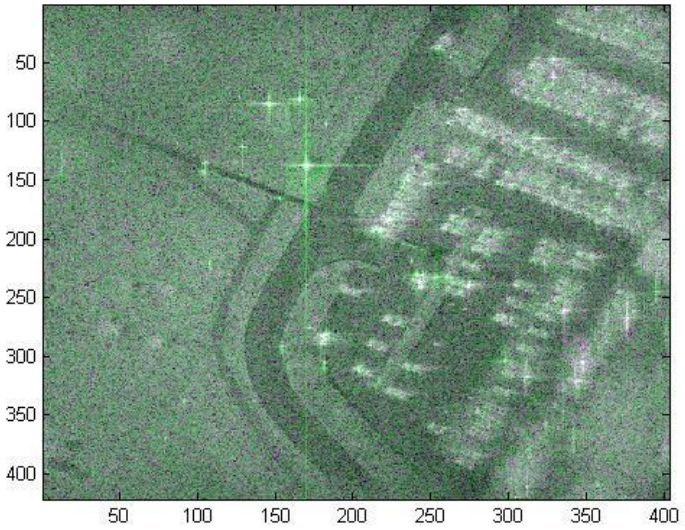

Figure 4.12: This is a SAR image using linear decomposition, obtained computing the SAR raw data from pass1, azimuth angle number 60 and RGB color space.

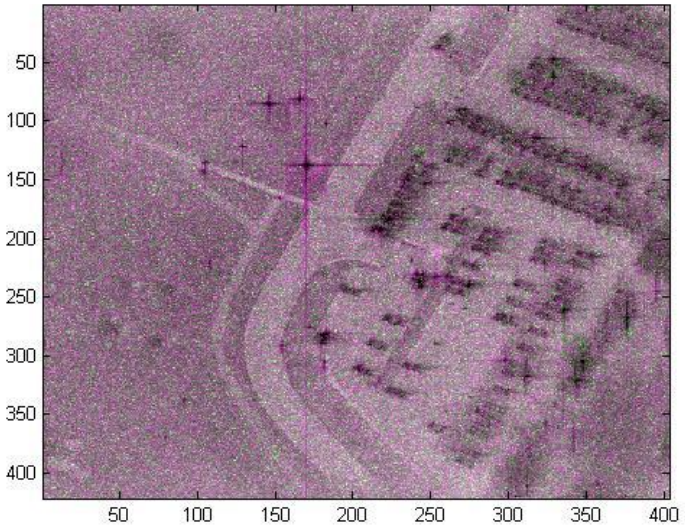

Figure 4.13: This is the same SAR image on Figure 4.12 but computed for CMY color space. The process of compute the CMY color space image is by subtracting the RGB values of Figure 4.12 from one.

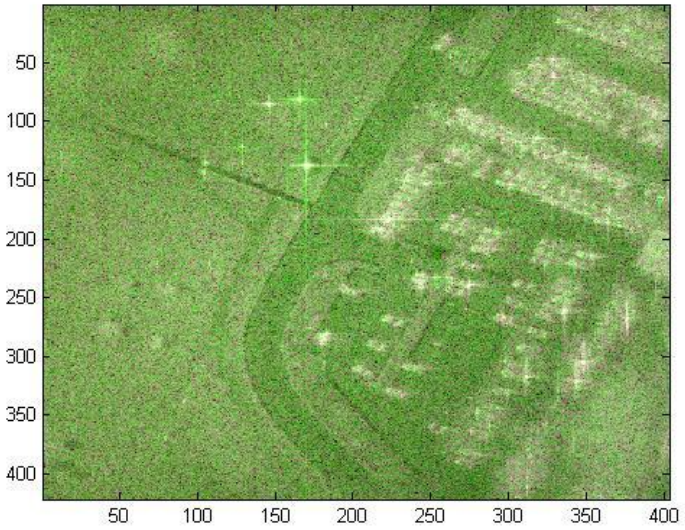

Figure 4.14: This is a SAR image using Pauli decomposition, obtained computing the SAR raw data from pass1, azimuth angle number 60 and RGB color space.

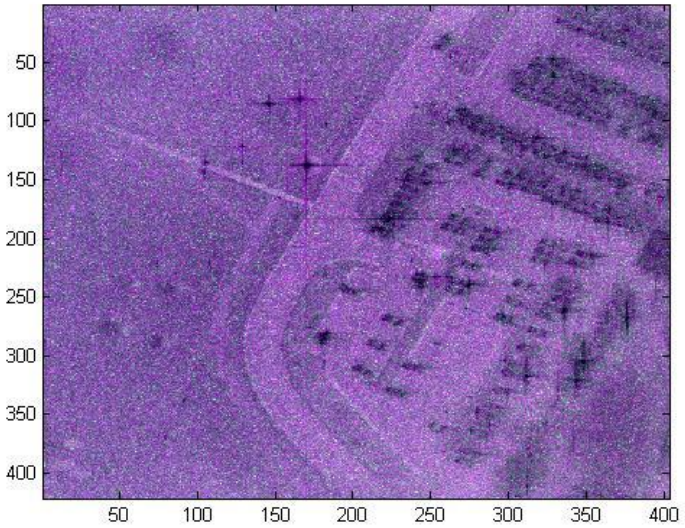

Figure 4.15: This is the same SAR image on Figure 4.14 but computed for CMY color space. The process of compute the CMY color space image is by subtracting the RGB values of Figure 4.14 from one.

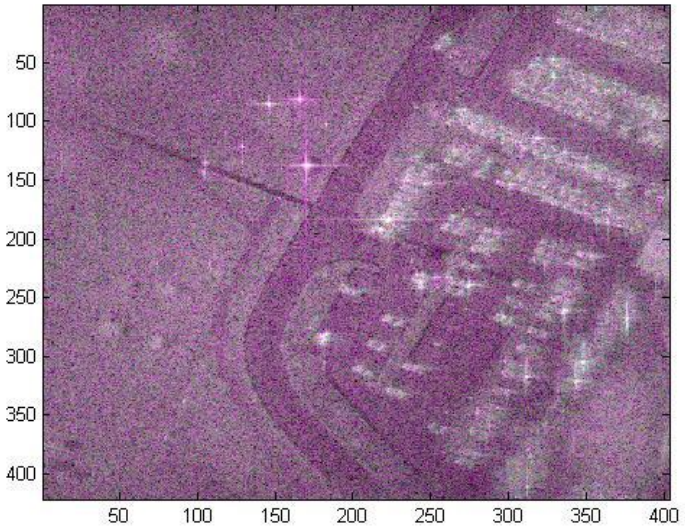

Figure 4.16: This is a SAR image using Krogager decomposition, obtained computing the SAR raw data from pass1, azimuth angle number 60 and RGB color space.

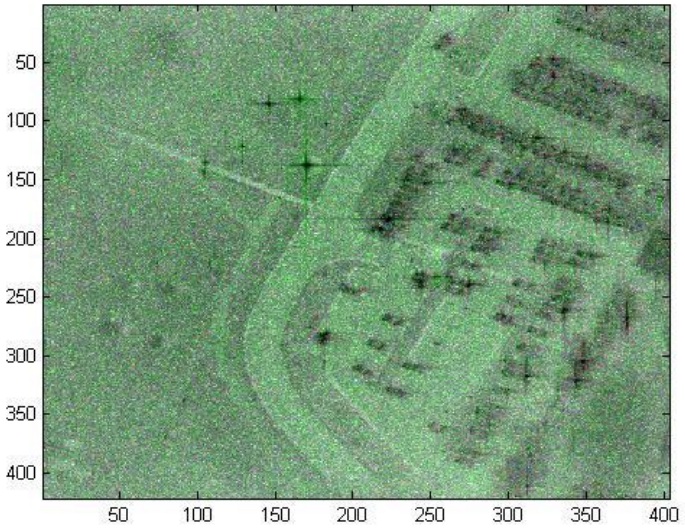

Figure 4.17: This is the same SAR image on Figure 4.16 but computed for CMY color space. The process of compute the CMY color space image is by subtracting the RGB values of Figure 4.16 from one.

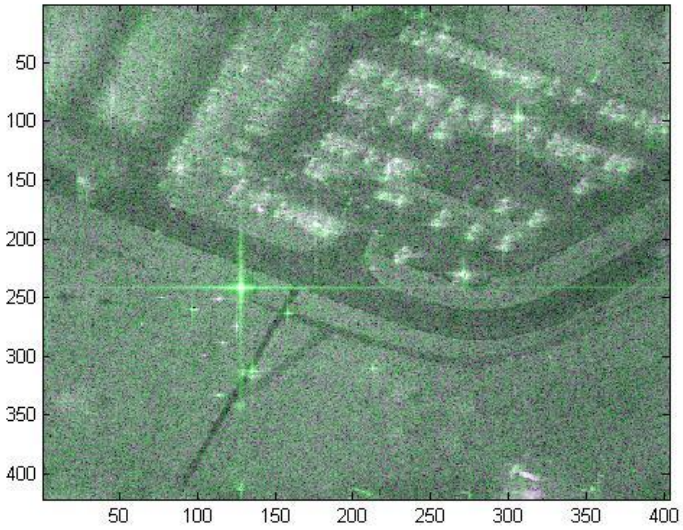

Figure 4.18: This is a SAR image using linear decomposition, obtained computing the SAR raw data from pass1, azimuth angle number 150 and RGB color space.

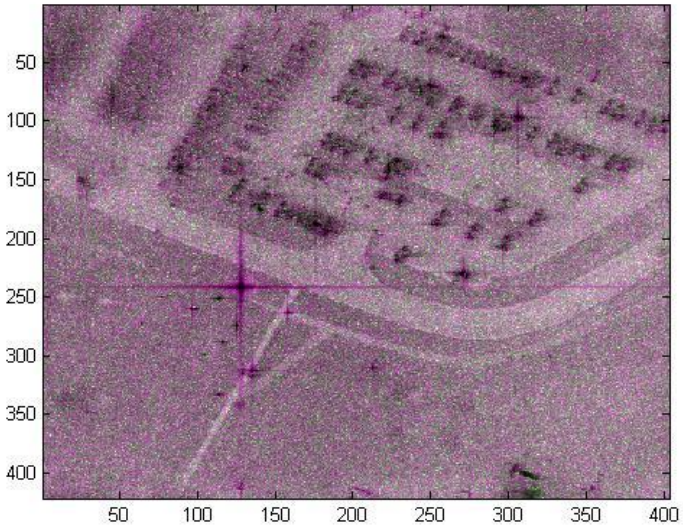

Figure 4.19: This is the same SAR image on Figure 4.18 but computed for CMY color space. The process of compute the CMY color space image is by subtracting the RGB values of Figure 4.18 from one.

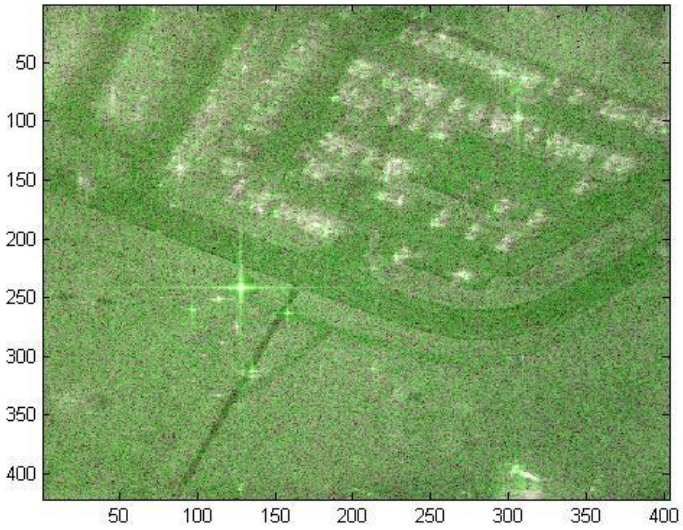

Figure 4.20: This is a SAR image using Pauli decomposition, obtained computing the SAR raw data from pass1, azimuth angle number 150 and RGB color space.

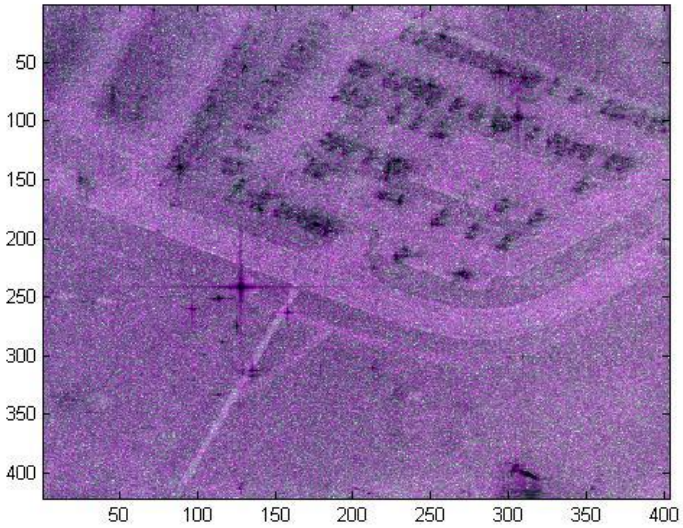

Figure 4.21: This is the same SAR image on Figure 4.20 but computed for CMY color space. The process of compute the CMY color space image is by subtracting the RGB values of Figure 4.20 from one.

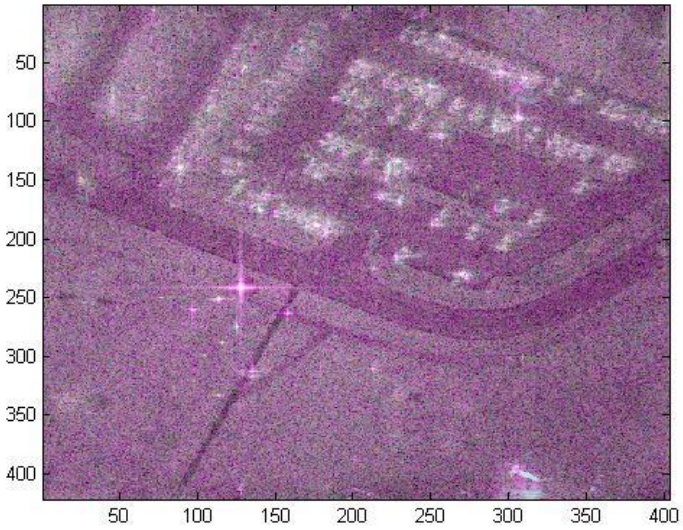

Figure 4.22: This is a SAR image using Krogager decomposition, obtained computing the SAR raw data from pass1, azimuth angle number 150 and RGB color space.

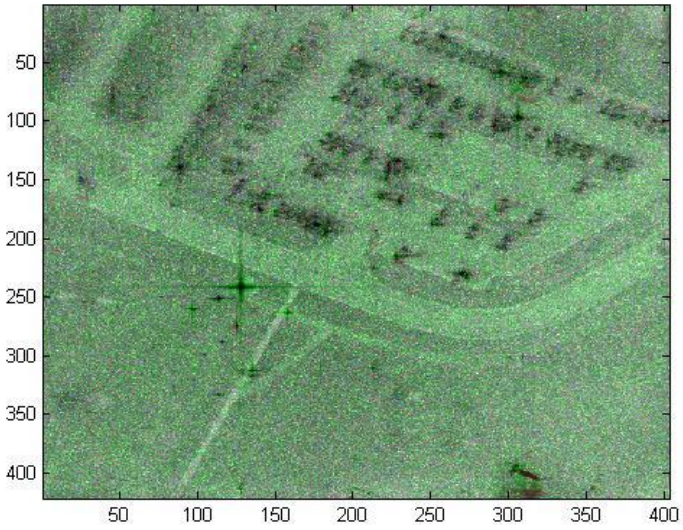

Figure 4.23: This is the same SAR image on Figure 4.22 but computed for CMY color space. The process of compute the CMY color space image is by subtracting the RGB values of Figure 4.22 from one.

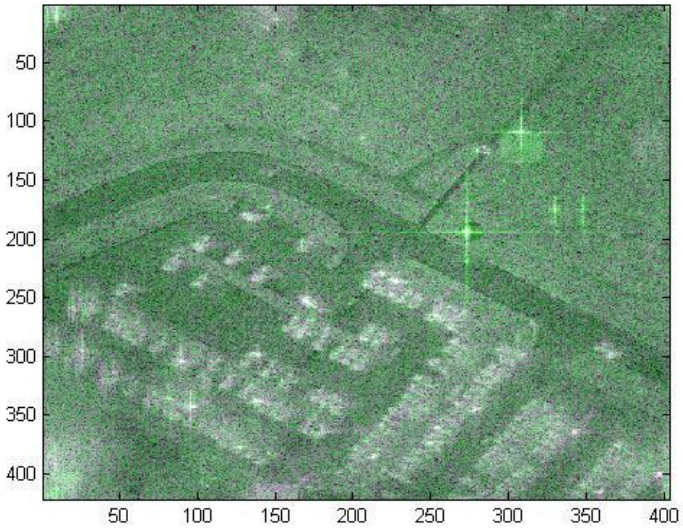

Figure 4.24: This is a SAR image using linear decomposition, obtained computing the SAR raw data from pass1, azimuth angle number 320 and RGB color space.

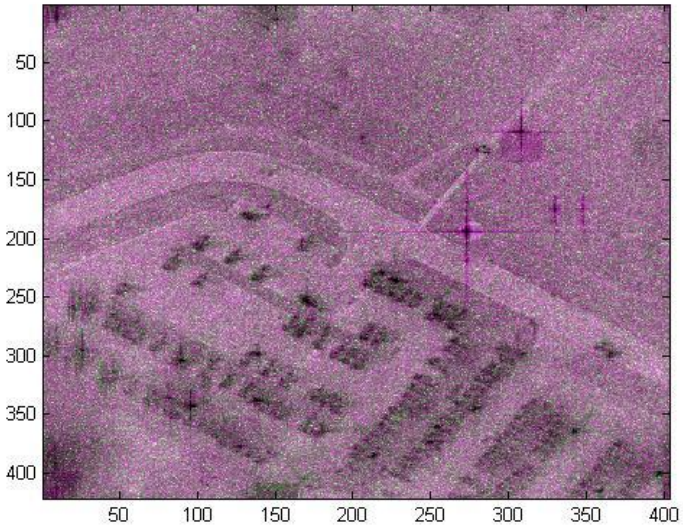

Figure 4.25: This is the same SAR image on Figure 4.24 but computed for CMY color space. The process of compute the CMY color space image is by subtracting the RGB values of Figure 4.24 from one.

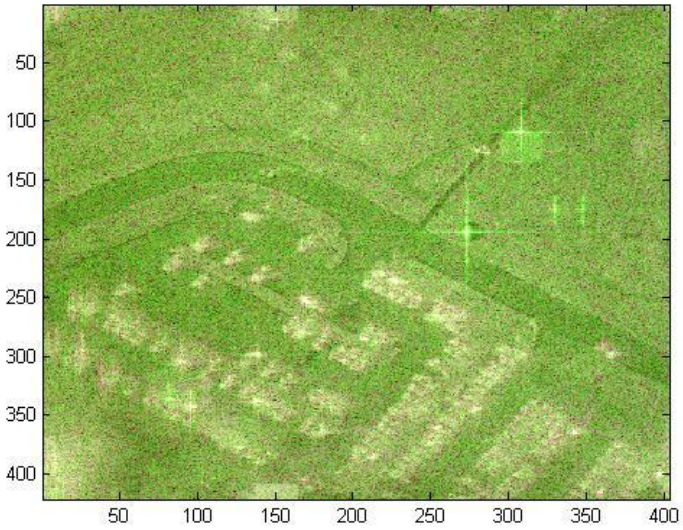

Figure 4.26: This is a SAR image using Pauli decomposition, obtained computing the SAR raw data from pass1, azimuth angle number 320 and RGB color space.

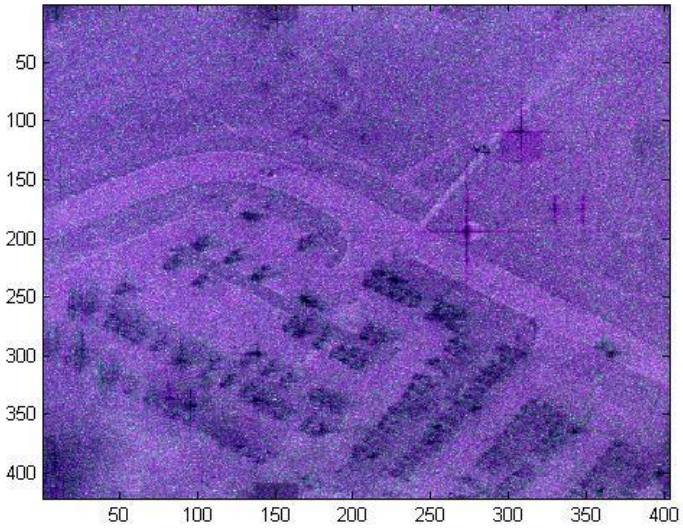

Figure 4.27: This is the same SAR image on Figure 4.26 but computed for CMY color space. The process of compute the CMY color space image is by subtracting the RGB values of Figure 4.26 from one.

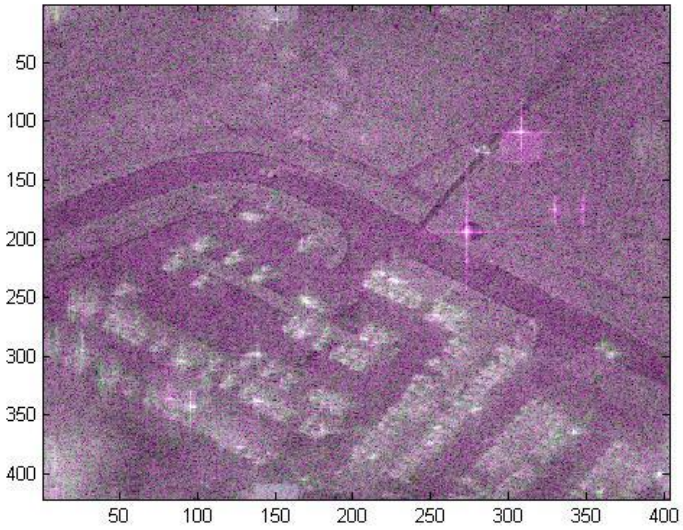

Figure 4.28: This is a SAR image using Krogager decomposition, obtained computing the SAR raw data from pass1, azimuth angle number 320 and RGB color space.

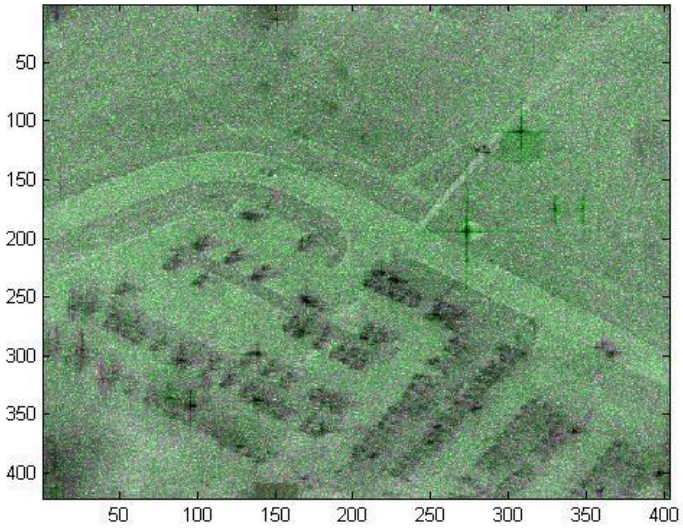

Figure 4.29: This is the same SAR image on Figure 4.28 but computed for CMY color space. The process of compute the CMY color space image is by subtracting the RGB values of Figure 4.28 from one.

In the case of linear decomposition and RGB color space for all the azimuth angles observed, as shown on Figures 4.6, 4.12, 4.18 and 4.24, the road can be easily

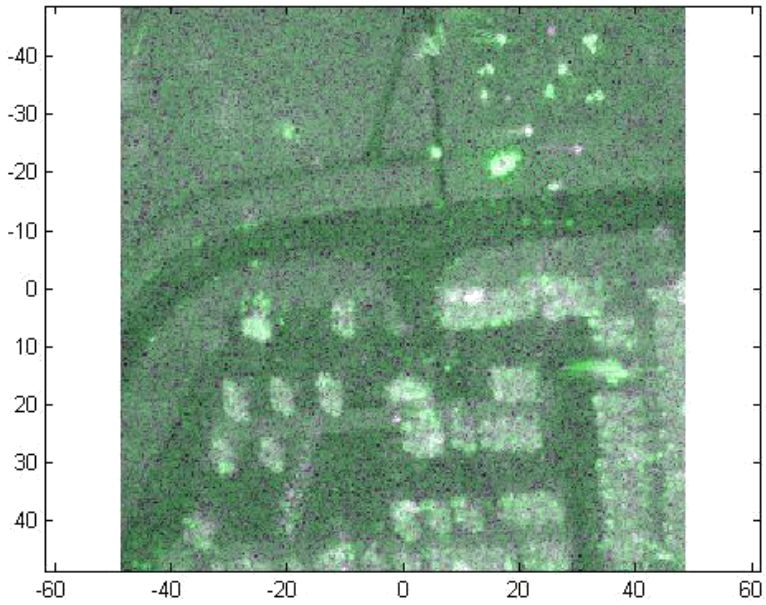

Figure 4.30: This is a SAR image using Linear decomposition, obtained computing the SAR raw data from pass1, full azimuth (360^o) and RGB color space.

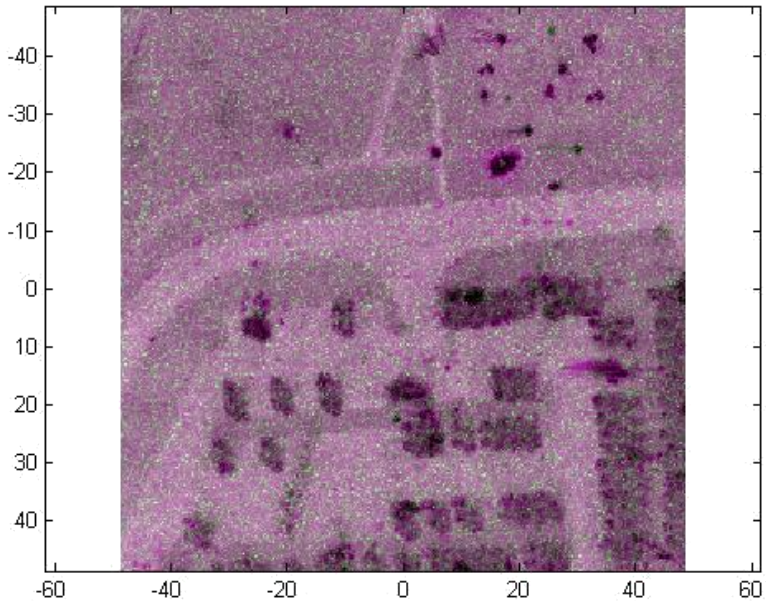

Figure 4.31: This is the same SAR image on Figure 4.30 but computed for CMY color space. The process of compute the CMY color space image is by subtracting the RGB values of Figure 4.30 from one.

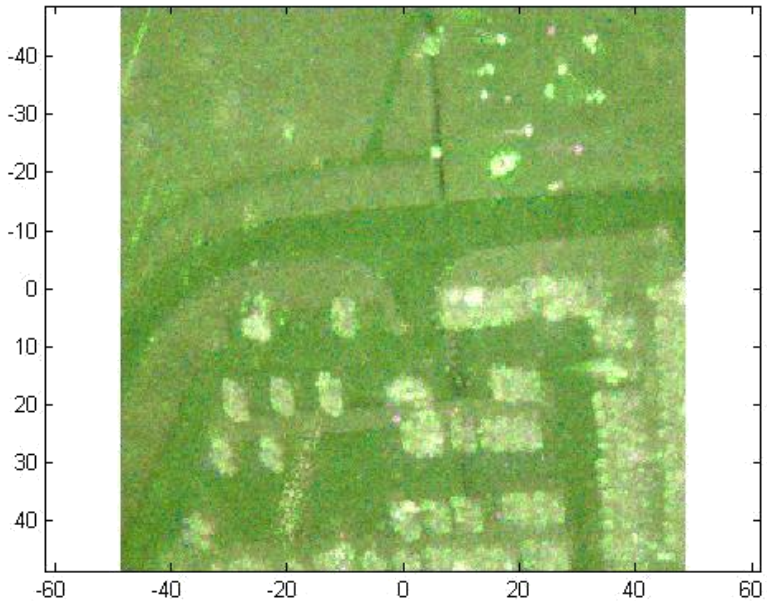

Figure 4.32: This is a SAR image using Pauli decomposition, obtained computing the SAR raw data from pass1, full azimuth (360^o) and RGB color space.

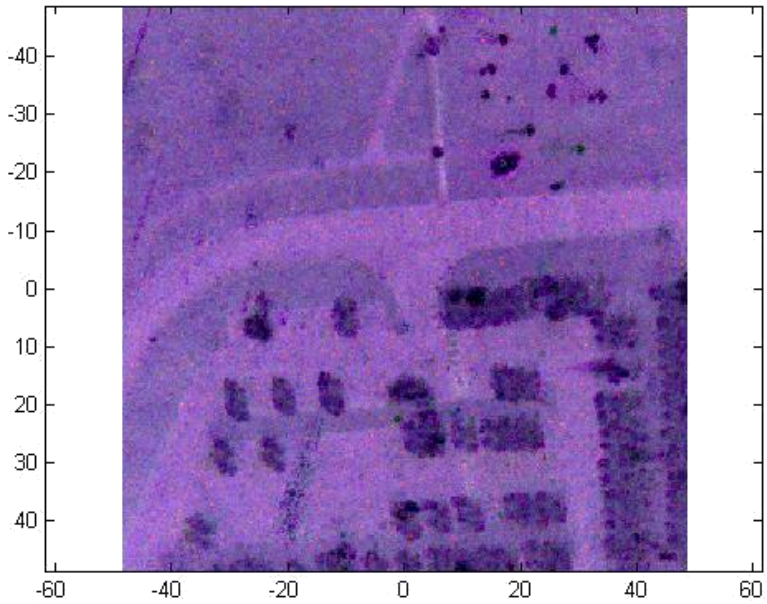

Figure 4.33: This is the same SAR image on Figure 4.32 but computed for CMY color space. The process of compute the CMY color space image is by subtracting the RGB values of Figure 4.32 from one.

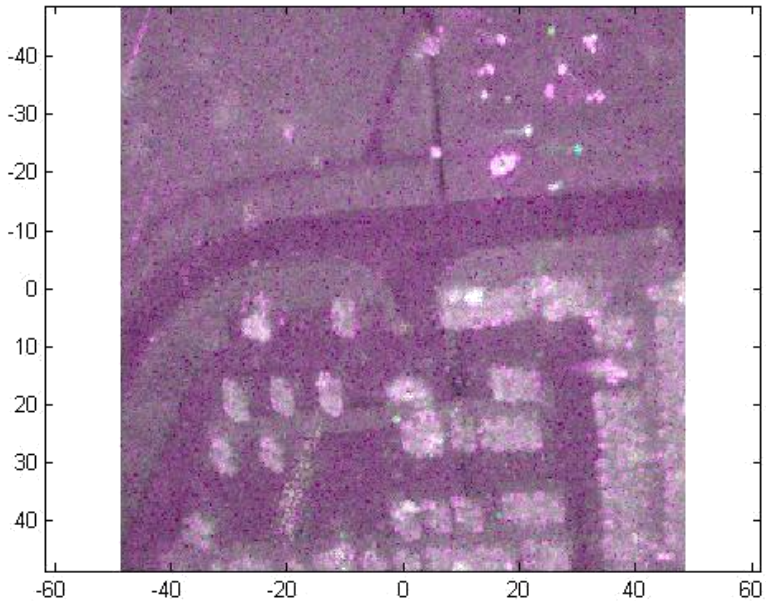

Figure 4.34: This is a SAR image using Krogager decomposition, obtained computing the SAR raw data from pass1, full azimuth (360^o) and RGB color space.

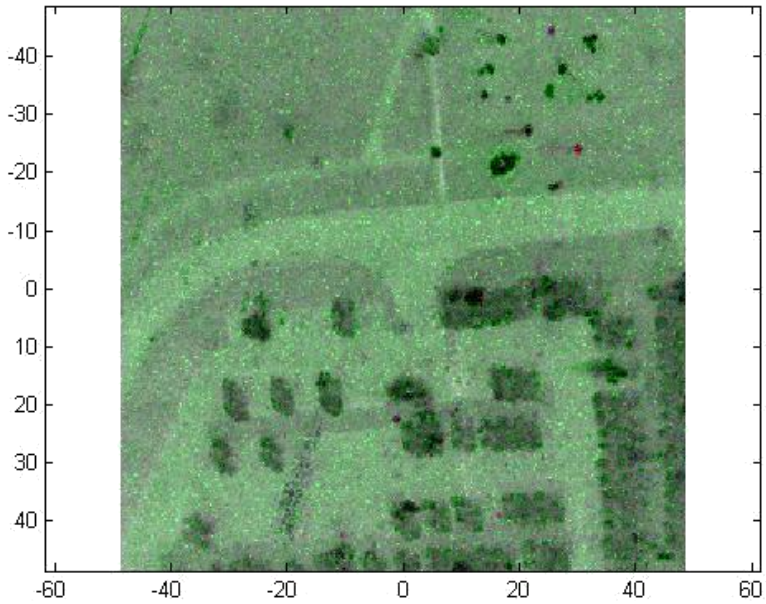

Figure 4.35: This is the same SAR image on Figure 4.34 but computed for CMY color space. The process of compute the CMY color space image is by subtracting the RGB values of Figure 4.34 from one.

noted and differentiated from the rest of the terrain, which, for this case represents the contribution of the cross-polarized scatter. The man-made objects present in the scene are denoted with color nearest to white, due to the contribution of S_{hh} and S_{vv} and S_{hv} or S_{vh} polarization channels. In other words, each polarization channel contributed with a high value for intensity, giving to each pixel a high contribution for each RGB color. Due to the additive nature of RGB color space, the resulting pixels shows up as a near to a white color for those elements.

In the case of linear decomposition and CMY color space for all the azimuth angles observed, as shown on Figures 4.7, 4.13, 4.19 and 4.25, the man-made objects present in this scene are displayed with darker color tones, due to the way that CMY color space were created, which is basically the complement of the RGB color space. The darker colors do not allow to an average observer like the author to distinguish sharper shapes of man-made objects as a result of the contribution of S_{hh} and S_{vv} polarization channels.

In the case of Pauli decomposition and RGB color space for all the azimuth angles observed, as shown on Figures 4.8, 4.14, 4.20 and 4.26, the road color tones are not noted as easily as the one in the linear decomposition SAR image still can be differentiated from the rest of the terrain, which, for this case represents the contribution of the cross-polarized scatter. The man-made objects present in the scene show intensity values higher than the ones from the linear decomposition [16, 19, 22] and according to an average observer, the man-made objects have sharper shapes than the linear decomposition technique. This is due to the algebraic way that the contribution of S_{hh} and S_{vv} polarization channels are related in the Pauli decomposition.

In the case of Pauli decomposition and CMY color space for all the azimuth angles observed, as shown on Figures 4.9, 4.15, 4.21 and 4.27, the scene in general is displayed with darker color tones, due to the way that CMY color space were created, and the effect that this color space has over the image is the same as the one in the

linear decomposition, degrading the perception of the shapes of man-made objects present in the scene.

In the case of Krogager decomposition and RGB color space for all the azimuth angles observed, as shown on Figures 4.10, 4.16, 4.22 and 4.28, the contrast between the road and the rest of the scene is much better, making it easier to recognize the road than in the other two decomposition techniques. The man-made objects present in the scene are not as sharp and clear as those from the linear decomposition and Pauli decomposition, this is due to the Krogager decomposition was created to highlight circular scatter present in the scene [2,15,16,19,22], which is not the main contribution of main made objects that are dominated by linear scatter.

In the case of Krogager decomposition and CMY color space for all the azimuth angles observed, as shown on Figures 4.11, 4.17, 4.23 and 4.29, the scene in general is displayed with darker color tones, due to the way that CMY color space were created, and the effect that this color space has over the image is the same as the one in the linear and Pauli decomposition, degrading the perception of the shapes of man-made objects present in the scene.

In general for all the azimuth angles observed, the effect of the change of color space from RGB to CMY color space for the three decomposition techniques is practically the same, from a perception point of view. This is CMY color space makes SAR imagery looks darker in general, making it harder to extract features for an average observer. This is due to the way that color space was computed, as explained in section 2.3.2.3.

In Figures 4.30 through 4.34 we can observe the result of adding all the contribution from all the azimuth angle for the Linear, Pauli and Krogager decomposition using RGB and CMY color spaces. The differences of features displayed for each decomposition can be observed.

V. Conclusion

5.1 Research Summary

This research provides a compilation SAR polarimetric fundamentals and shows how multi-color imagery can be constructed using raw SAR data. Three decomposition techniques (linear, Pauli, Krogager) and their relationship with color spaces for SAR multi-color imagery were considered. The effects of using these three scattering matrix decomposition techniques and two different color spaces (RGB and CMY) are shown when constructing multi-color SAR imagery from sparse data, i.e. low resolution data. Examples of SAR images based on linear, Pauli and Krogager decompositions were presented.

According to [12], for an electronic imaging device, there are some desirable characteristics for color spaces. One of them is that the color space needs to be device independent, with coordinates that are measurable and related to the standard observer. These characteristics are clearly opposite to the hypothesis that originates this research which considers device-dependent color spaces. Color spaces like RGB and CMY were generally designed for specific devices, e.g. computer monitors and television are RGB-based and color printers are CMY-based. Is necessary to say that, during the simulation process, the only way to compute a SAR image in a CMY color space was by subtracting the RGB vector value from one. In color language, this means subtracting RGB from white to obtain the equivalent color in the CMY color space. In this case, the resultant format remains RGB and the image can be displayed using a monitor in the RGB color space.

Considering that one of the research objectives was to establish a performance metric for comparing between combinations of decomposition technique and color space, a deep literature review was conducted in color science and the way that humans sense color stimulus. After considering all information obtained from this literature review, the following conclusions were made;

- Since this research was oriented to determine how different comobination of color space and decomposition technique could improve feature extraction for

an observer or analyst, performance depends directly upon the observer since every human senses and interprets color stimuli differently;

- Sensing a particular color depends not only on the way the color is stimulating the sensor, which for the human case is the eye, but also on the environment, available light and contrast at which the color is being displayed;
- If all the electronic devices on which the image is to be displayed are not calibrated and not working under the same conditions, the image perception can be different, stimulating the sensor differently, and hence obtaining a different interpretation of information from the same image;
- RGB color space is an additive space where different colors are obtained by adding the fundamental colors of Red, Green and Blue with different intensity weights, with the white color obtained by adding all three colors at their maximum value;
- CMY color space is a subtractive color space where the different colors are obtained by absorbing the reflections, i.e., when Cyan and Magenta colorants are mixed, cyan absorbs the red reflection of the magenta and magenta absorbs the green reflection of cyan. This leaves blue as the only non-absorbing region.
- When color spaces are used to construct multi-color SAR images, each color is mapped to one of the three layers that form part of the decomposed SAR image. The intensity for that color in a particular pixel at each layer is given by the addition of the contribution of the three layers in the respective pixels.
- The intensity value of each SAR image pixel is independent of the color space used in SAR imagery.
- Considering that there is not a mathematical definition for RGB and CMY color spaces that can be used to compare them from a performance point-of-view, the only performance that could be analyzed was variation in decomposition technique.

- Decomposition techniques were created to extract different features and highlight different elements in a scene from the electromagnetic point-of-view.

Considering all factors described above, there was one method used to quantitatively determines performance of the three decompositions. The method was based on estimating shift values of a pixel image in the vertical and horizontal coordinates based upon the features present in each image. Even though both images look similarly, each of them were generated in order to show different characteristics of the same scene.

5.2 Contributions.

- At the beginning of this research, AFIT has no tools and experience on computing Multi-Color polarimetric SAR imagery. With this thesis, a tool for computing Multi-Color Polarimetric SAR imagery is available as a Matlab Code for Masters or PhD researchers that can take this research to the next level;
- The thesis as a written document compiles the fundamentals on SAR Polarimetry, Color Spaces and Multi-Color SAR imagery that will give to future researchers on this area a good starting point for further research;
- The Gotcha data set was released as a Challenge to the SAR community in order to explore the 3-dimensional SAR imaging problem. This thesis explore a different angle of the Gotcha data set being the first research to approach the data set to build Multi-Color polarimetric imagery. Hence, this thesis could complement the 3-dimensional approach in order to improve feature extraction or target recognition capabilities using polarimetric SAR.

5.3 Suggestions for Further Research.

This research can be used as a tutorial for polarimetric SAR imaging, since the fundamentals of SAR polarimetry are discussed in detail in Chapter II. During the development of this research, polarimetric SAR, scattering matrix decomposition and

graphical representation were explained as well as the relationship with the RGB and CMY color spaces in Chapter III. Now days, there is a great variety of color spaces and new methods for computing color in electronic devices. These could be further analyzed in order to identify color space or a method for improving the way that SAR polarimetry data is displayed to operators. In this way, feature extraction can be made in a more efficient and accurate way.

Two specific decomposition techniques were explored, and there is a great variety available for the SAR community to analyze. This might be a good opportunity to expand the analysis made under this research.

The code to compute multicolor polarimetric SAR imagery was under constant development. During the later stages of this research, a Dynamic Range normalization was performed in order to improve the quality of the imagery obtained. After considering different approaches to this problem, it become evident that, as the center value of the dynamic range varies, differences occured in the features presented for each image. This highlight that different types of scatterers, i.e., volumetric or man-made, might be used as a discriminator if the feature of interest are known a-priori.

Bibliography

1. *GOTCHA 2D/3D Imaging Challenge Problem AFRL/SNAS*. Technical report, Air Force Research Laboratory, United States Air Force, 2007.

2. Alberga, V., E. Krogager, M. Chandra, and G. Wanielik. "Potential of Coherent Decompositions in SAR Polarimetry and Interferometry". *Geoscience and Remote Sensing Symposium, 2004.IGARSS'04. Proceedings.2004 IEEE International*, volume 3, 1792–1795 vol.3. Sept. 2004.

3. Boerner, W.-M. and H. berall. *Radar Target Imaging*. Springer'Verlag, Berlin Heidelberg, 1994.

4. Curtis H. Casteel, Jr., LeRoy A. Gorham, Michael J. Minardi, Steven M. Scarborough, Kiranmai D. Naidu, and Uttam K. Majumder. "A challenge problem for 2D/3D imaging of targets from a volumetric data set in an urban environment". volume 6568, 65680D. SPIE, 2007.

5. Ertin, E., C. D. Austin, S. Sharma, R. L. Moses, and L. C. Potter. "GOTCHA experience report: three-dimensional SAR imaging with complete circular apertures". *Algorithms for Synthetic Aperture Radar Imagery XIV. Edited by Zelnio, Edmund G.; Garber, Frederick D.. Proceedings of the SPIE, Volume 6568, pp. 656802 (2007).*, volume 6568 of *Presented at the Society of Photo-Optical Instrumentation Engineers (SPIE) Conference*. April 2007.

6. Gonzalez, Rafael C. and Richard E. Woods. *Digital Image Processing*. Pearson Prentice Hall, Upper Saddle River, NJ, 2008.

7. Hunt, R.W.G. "Application of a Model of Color Appearance to Practical Problems in Imaging". volume 90. January 2002.

8. H.V.Poor. *Introduction of Signal Detection and Estimation, 3rd Edition*. Springer, New York, NY, 1994.

9. Ibarra, C., O. Kegege, Junfei Li, and H. Foltz. "Radar Polarimetry for Target Discrimination". *Region 5 Technical Conference, 2007 IEEE*. 2007.

10. Inglada, J., J.-C. Souyris, C. Henry, and C. Tyson. "Incoherent SAR Polarimetric Analysis over Point Targets". volume 3, 246–249. April 2006.

11. Jakowatz, Charles V., Daniel E. Wahl, Paul H. Eichel, Dennis C. Ghiglia, and Paul A. Thompson. *Spotlight-mode Synthetic Aperture Radar: A Signal Processing Approach*. Kluwer Academic Publishers, Boston MA, 1996.

12. Kang, Henry R. *Color Technology for Electronic Imaging Devices*. SPIE Optical Engineering Press, Bellingham, Washington, 1996.

13. Karim E. Mattar, Chen Liu and Ramin Sabry. *Polarimetric SAR Interferometry:Investigation using EC CV-580 SAR data*. Technical report, Canada Center for Remote Sensing, 2005.

14. Kim, Yunjin and J. Van Zyl. "Overview of Polarimetric Interferometry". *Aerospace Conference Proceedings, 2000 IEEE*, volume 3, 231–236 vol.3. 2000.

15. Krogager, Ernst. "Advances of Techniques for Utilizing Polarimetric Features of Radar Targets". *2004 Target Identification and Recognition Using RF Systems Symposium*. 2006.

16. Lee, Jong-Sen and Eric Pottier. *Polarimetric Radar Imaging*. CRC Press, Boca Raton, FL, 2009.

17. Ltd., Intermap Technologies. *Fundamental of Remote Sensing*. Technical report, Canada Center for Remote Sensing, 2005.

18. Malacara, Daniel. *Color Vision and Colorimetry: Theory and Applications*. SPIE Press, Bellingham, WA, 2002.

19. Massonnet, Didier and Jean-Claude Suyris. *Imaging with Synthetic Aperture Radar*. EPFL Press, Boca Raton, FL, 2008.

20. Matson, Charles and Alim Haji. "Biased Cramer-Rao lower bound calculations for inequality-constrained estimators". *AFRL-DE-PS-JA-2007-1011, Air Force Research Laboratory*, September 2006.

21. Minkoff, John. *Signal Processing Fundamentals and Applications for Communications and Sensing Systems*. Artech House Inc., Norwood, MA, 2002.

22. Mott, Harold. *Polarimetric Radar*. John Wiley & Sons, Inc., Hoboken NJ, 2007.

23. Reck, M. and G. Schreier. "Fourier Series Representation of SAR Polarimetric Scattering Signatures". *Geoscience and Remote Sensing Symposium, 1990.IGARSS'90.'Remote Sensing Science for the Nineties'.,10th Annual International*. 1990.

24. Richards, Mark A. *Fundamentals of Radar Signal Processing*. McGraw-Hill, Hoboken NJ, 2005.

25. Robinson, D. and P. Milanfar. "Fundamental Performance Limits in Image Registration". volume 13, 1185–1199. Sept. 2004.

26. Sadjadi, F. "Improved Target Classification using Optimum Polarimetric SAR Signatures". *Aerospace and Electronic Systems, IEEE Transactions on*, 38(1):38–49, Jan 2002.

27. Skolnik, Merrill I. *Introduction to Radar Systems*. McGraw Hill, Boston MA, 2001.

28. Soumekh, Mehrdad. *Synthetic Aperture Radar Signal Processing with MATLAB Algorithms*. John Wiley & Sons, Inc., New York NY, 1999.

29. Tkalcic, M. and J.F. Tasic. "Color Spaces: Perceptual, Historical and Applicational Background". volume 1, 304–308 vol.1. Sept 2003.

30. Valberg, Arne. *Light Vision Color*. John Wiley & Sons Ltd,, West Sussex, England, 2005.

31. Wyszecky, Gunter and W.S.Stiles. *Color Science:Concepts and Methods, Quantitative Data and Formulae, Second Edition*. John Wiley & Sons, Inc., New York, NY, 1982.

32. Xie, Hua, L.E. Pierce, and F.T. Ulaby. "Mutual information based registration of SAR images". *Geoscience and Remote Sensing Symposium, 2003.IGARSS'03. Proceedings.2003 IEEE International*. 2003.

33. Zheng, Li, Jianqing Zhang, and Yuejun Luo. "Color Matching in Colour Remote Sensing Image". volume 3, 303–306. June 2006.

REPORT DOCUMENTATION PAGE

Form Approved
OMB No. 0704–0188

1. REPORT DATE *(DD–MM–YYYY)*	2. REPORT TYPE	3. DATES COVERED *(From — To)*
25–03–2010	Master's Thesis	September 2008 – March 2010

4. TITLE AND SUBTITLE

Performance of Scattering Matrix Decomposition and Color Spaces for Synthetic Aperture Radar Imagery.

5a. CONTRACT NUMBER

5b. GRANT NUMBER

5c. PROGRAM ELEMENT NUMBER

6. AUTHOR(S)

Arriagada, Manuel E., Captain, Chilean Air Force

5d. PROJECT NUMBER

09EN135

5e. TASK NUMBER

5f. WORK UNIT NUMBER

7. PERFORMING ORGANIZATION NAME(S) AND ADDRESS(ES)

Air Force Institute of Technology
Graduate School of Engineering and Management (AFIT/EN)
2950 Hobson Way
WPAFB OH 45433-7765 DSN: 785-3636

8. PERFORMING ORGANIZATION REPORT NUMBER

AFIT/GE/ENG/10-03

9. SPONSORING / MONITORING AGENCY NAME(S) AND ADDRESS(ES)

Mr Tom Lewis, Gotcha Systems Engineer
937.255.6427 x4347, thomas.lewis3@wpafb.af.mil
RF Systems & Analysis Branch, Sensors Directorate, Air Force Research Laboratory
Bldg 620, 2241 Avionics Circle, Wright-Patterson Air Force Base, OH 45433

10. SPONSOR/MONITOR'S ACRONYM(S)

AFRL/RYRR

11. SPONSOR/MONITOR'S REPORT NUMBER(S)

12. DISTRIBUTION / AVAILABILITY STATEMENT

APPROVAL FOR PUBLIC RELEASE; DISTRIBUTION IS UNLIMITED.

13. SUPPLEMENTARY NOTES

14. ABSTRACT

Polarization decomposition techniques are applied to the polarization-dependent data to form colorful imagery that is easy for a human to interpret. Yet, the presumption is that the SAR system operates with maximum bandwidth requiring extensive processing for near- or real-time application. In this thesis, the author investigates the differences between the choices of color space when processing sparse SAR data with three scattering matrix decompositions (linear, Pauli and Krogager) to determine the best combination for accurate feature extraction. Hence, SAR imagery was computed for the combination of decomposition techniques and color spaces. This set of SAR imagery allows the reader to have an abstract idea of the differences between the combination of decomposition techniques and color spaces.

15. SUBJECT TERMS

SAR, Polarimetric SAR, Color Spaces.

16. SECURITY CLASSIFICATION OF:			17. LIMITATION OF ABSTRACT	18. NUMBER OF PAGES	19a. NAME OF RESPONSIBLE PERSON
a. REPORT	b. ABSTRACT	c. THIS PAGE			Major Michael A. Saville (ENG)
U	U	U	UU	88	19b. TELEPHONE NUMBER *(include area code)* (937) 255-3636 x4719 - Michael.Saville@afit.edu